Article

Mural cells protect the adult brain from hemorrhage but do not control the blood-brain barrier in developing zebrafish

Oguzhan F Baltaci[1,2,#], Andrea Usseglio Gaudi[1,2], Stefanie Dudczig[1,2], Weili Wang[3], Scott Paterson[1,2], Maria Cristina Rondon-Galeano[1,2], Ye-Wheen Lim[3], James Rae[3], Anne Lagendijk[3], Robert G Parton[3,6], Alison Farley[1,2,4], Benjamin M Hogan[1,2,5,#]

[1] Organogenesis and Cancer Program, Peter MacCallum Cancer Centre, Melbourne, VIC 3000, Australia.
[2] Sir Peter MacCallum Department of Oncology, University of Melbourne, Melbourne, VIC 3000, Australia.
[3] Institute for Molecular Bioscience, The University of Queensland, St Lucia, 4072, QLD, Australia
[4] Walter and Eliza Hall Institute of Medical Research, Melbourne, Victoria 3052, Australia.
[5] Department of Anatomy and Physiology, University of Melbourne, Melbourne, VIC 3000, Australia.
[6] Centre for Microscopy and Microanalysis, The University of Queensland, St Lucia, 4072, QLD, Australia

[#] *Authors for Correspondence:*

Professor Ben Hogan & Dr Oguzhan Baltaci
Organogenesis and Cancer Program,
Peter MacCallum Cancer Centre,
Melbourne, VIC 3000, Australia
E-mail: ben.hogan@petermac.org &/or oguzhan.baltaci@petermac.org

Abstract

The blood-brain barrier (BBB) protects the brain from circulating metabolites and plays central roles in neurological diseases. Endothelial cells (ECs) of the BBB are enwrapped by mural cells including pericytes and vascular smooth muscle cells (vSMCs) that regulate angiogenesis, vessel stability and barrier function. To explore mural cell control of the BBB, we investigated neurovascular phenotypes in zebrafish *pdgfrb* mutants that lack brain pericytes and vSMCs. As expected, mutants showed an altered cerebrovascular network with mispatterned capillaries. Unexpectedly, mutants displayed no BBB leakage at larval stages of development. This demonstrates that pericytes and vSMCs do not control BBB function in developing zebrafish. Instead, we observed juvenile and adult BBB disruption occurring at "hotspot" focal hemorrhages at large vessel aneurysms. ECs at leakage hotspots showed induction of caveolae on abluminal surfaces and structural defects including basement membrane thickening and disruption. Our work suggests that capillary pericytes regulate cerebrovascular patterning in development and vSMCs of major arteries protect from hemorrhage and BBB breakdown in older zebrafish. The fact that young zebrafish have a functional BBB in the absence of mural cells calls for renewed interrogation of mural cell control of the BBB throughout vertebrate evolution.

Introduction

Mammalian neurovascular endothelial cells (ECs) have unique functional and structural properties to regulate substance exchange between the blood and the brain, establishing the blood-brain barrier (BBB)[1,2]. Loss of normal BBB function is associated with neuropathological states, including neurodegeneration, infection and cancer[1,2]. Mural cells are vascular support cells that include pericytes and vascular smooth muscle cells (vSMCs) and control vascular development, function and BBB permeability[3-9]. PDGFB/PDGFRβ signaling is required for the development of mural cells[3,4,10-12] and their depletion in PDGFB- or PDGFRβ-deficient rodents causes altered angiogenesis, aneurysm and vessel leakiness[3-6,13]. Strikingly, rodent models of pericyte loss have an open BBB, with free transport of tracer dyes from the blood stream into the brain parenchyma but an otherwise intact vasculature[5,6]. These and other observations have led to a current model whereby pericytes control BBB function by suppressing EC transcytosis, via a mechanism not yet fully understood. Such a mechanism holds significant translational promise to safely "open" the BBB in therapeutic settings, by discovering ways to disrupt pericyte control of ECs[5,14].

Studies of the BBB using invertebrates like *Drosophila* and some basal vertebrate fishes (e.g. some *Elasmobranchii* and *Chondrostei*) have suggested that the makeup of the BBB can vary

81 significantly across the phylogeny. These species display a primarily glial cell barrier, rather
82 than an EC barrier[15,16]. However, in the modern teleost *Danio rerio* (zebrafish) the BBB cellular
83 composition is more similar to that seen in mammals[17-21]. As in mammals, the zebrafish BBB
84 is controlled by tightly adherent vascular ECs that share many characteristics with the ECs of
85 the mammalian brain. Zebrafish BBB endothelium expresses conserved molecular markers
86 (e.g. *glut1, cldn5, mfsd2a*)[18,20-23] and displays similar tight cell-cell junctions as observed at
87 the mammalian BBB[17,20,22]. The membrane transport protein Mfsd2a has been suggested to
88 have a conserved role in control of BBB function in zebrafish and mice[21,24], likely acting to
89 reduce the transfer of substances between bloodstream and parenchyma by suppressing EC
90 transcytosis[25,26]. Furthermore, during development the mechanisms that control the formation
91 of BBB ECs appear to show a high level of conservation between zebrafish and mice. Recent
92 studies have identified major roles for Wnt–β-catenin signaling, brain EC specific MMPs,
93 Vegfs and chemokine signaling in early BBB vascular EC development[23,27-29].

94 After the initial development of zebrafish BBB vasculature, mural cell populations develop and
95 mature. Transcriptionally, developing pericytes and vSMCs express many genes that are
96 highly conserved with mammals, for example zebrafish pericytes express well known markers
97 such as *pdgfrb, kcne4* and *abcc9* [30]. As in mice, *pdgfrb* mutants fail to form brain pericytes,
98 exhibit loss of vSMCs and display aneurysms as adults[13,31]. As well as conserved *pdgfrb*
99 control of mural cell development, Notch signaling[32] also plays a role in mural cell development
100 in zebrafish and in mice, with Notch 1 and 3 controlling the formation of pericytes in mice and
101 Notch 2 and Notch 3 paralogues important in zebrafish[33,34]. Overall, studies have suggested
102 a high level of conservation of the molecular control of mural cell development, yet how mural
103 cells control BBB function has not been interrogated in detail in zebrafish.

104 BBB function is first established in zebrafish between 3 days post fertilization (dpf, no barrier)
105 and 5 dpf (established barrier)[21]. During this period, developing mural cells (pericytes and
106 vSMCs) are establishing and expanding their interactions with brain ECs[31,34,35]. The first glial
107 cell neurovascular interactions are also observed during this period[36]. Throughout subsequent
108 larval, juvenile and adult development vSMC, pericyte and glial cell coverage of the
109 vasculature increases[31,36,37]. This is similar to mammals, albeit with some differences in the
110 relative timing that lineages arise, and the percentage of coverage of neurovasculature by
111 pericytes and glia may be lower in zebrafish. In mammals, microglia are known to play
112 important roles in the control of the BBB and neurovascular unit[38]. Zebrafish have a
113 microglial/macrophage population, but it is yet to be explored in detail in the control of the
114 BBB[39-41] and differences in other innate immune cells in the CNS has been recently reported[42].

115 Overall, while there are some areas remaining to be fully explored, the development, cellular
116 composition and the central role of ECs in the control of the zebrafish BBB is very similar to
117 mammals. As such, zebrafish are accepted as a highly accessible model to study BBB function,
118 as well as mural cell control of the BBB, relevant to mammalian biology[19].

119 Here, we explored mural cell control of BBB function in zebrafish. We used *pdgfrb* mutants
120 with loss of both pericytes and vSMCs, coupled with carefully optimized intravascular tracer
121 dye injections. We analyzed barrier function from developmental to adult stages and found
122 that at larval stages up to 14 dpf, well after the establishment of the BBB, loss of mural cells
123 does not lead to measurable BBB leakage or loss of BBB integrity. In adult animals, we
124 observed loss of BBB integrity that was consistent with leakage at hotspots, found to be
125 aneurysm associated hemorrhages. These hotspots were also observed in juvenile animals
126 (1 month old) and appeared to increase in number as animals aged. Our observations provide
127 no definitive evidence of BBB leakage at capillary networks that might be consistent with a
128 broad increase in EC transcytosis or loss of barrier integrity independent of focal hemorrhages.
129 This work demonstrates that young animals can have a functional BBB in the absence of mural
130 cells and highlights the central role for the EC in control of barrier function across the zebrafish
131 neurovasculature.

132 **Results**

133 To investigate the influence of mural cells upon the neurovasculature, we generated a *pdgfrb*
134 mutant (*pdgfrb*^{uq30bh}, hereafter *pdgfrb*$^{-/-}$), which possesses an early deletion leading to a
135 frameshift, predicted to cause a premature stop codon and a putative null allele (**Extended**
136 **Data Fig. 1a**). Using both the *TgBAC(pdgfrb:EGFP)*^{uq15bh} and *TgBAC(abcc9:abcc9-T2A-*
137 *mCherry)*^{um139} transgenic marker strains, we observed that pericytes were lost in the cerebral
138 central arteries of *pdgfrb* mutants (**Fig. 1a**, **Extended Data Fig. 1b–c**), as observed in
139 previous studies[13,31]. These mutants showed indistinguishable development from their wild-
140 type siblings up to 30 days post fertilization (dpf) and progressively reduced survival and
141 craniofacial defects thereafter (**Extended Data Fig. 1d–f**), consistent with previous studies of
142 *pdgfrb* null loss-of-function mutants[13,35]. To assess how brain vasculature develops without
143 pericytes, we imaged, traced and quantified central arteries in the midbrain (**Fig. 1a–c**). At 7
144 dpf, mutants displayed significantly reduced vascular complexity compared to siblings, with
145 reduced vessel length and branch points (**Fig. 1d–e**). This was more severe at 14 dpf,
146 demonstrating the phenotype is progressive (**Fig. 1d–e**). Timecourse imaging revealed the
147 reduction in vascular complexity was apparent from 5 dpf (**Fig. 1f–g**). These results suggest

148 that the pericytes (as vSMCs mature after 5 dpf[34]) regulate cerebral angiogenesis or
149 remodeling from early in larval development.

150 We next tested BBB function in mutants at 7 and 14 dpf. We performed intravenous injection
151 of fluorescently conjugated tracers of various molecular weights (1-kDa NHS, 10- and 70-kDa
152 Dextran), and live imaged fish at 2 hours post injection (hpi, the same timing used in[21])
153 (**Extended Data Fig. 2a**). 2000-kDa Dextran was co-injected to normalize for the amount of
154 vascular tracer delivered in each animal, and we measured intravascular versus extravascular
155 tracer intensity to assess leakage (see methods for full details). In control animals,
156 quantification confirmed that 2000-kDa tracer remained stably within the vasculature, while 1
157 kDa and 10 kDa were more readily detected in the brain parenchyma and 70 kDa provided
158 intermediate sensitivity (**Extended Data Fig. 2b–c**). This validated the use of 2000-kDa tracer
159 to normalize for amount of tracer injected, as reported elsewhere[43]. To provide additional
160 confidence in our measurements, we also normalized the extravasated tracer intensity to the
161 EC marker *kdrl* (*Tg(kdrl:EGFP)*^{s843} *or Tg(kdrl:Hsa.HRAS-mCherry)*^{s916}). We found no evidence
162 of elevated 10- or 70-kDa Dextran tracer extravasation into the brain parenchyma of *pdgfrb*
163 mutants compared to siblings at either timepoint (7 or 14 dpf) using any of our normalization
164 methods (**Fig. 2a–d**, **Extended Data Fig. 3a–d**). To confirm that our quantification methods
165 were sufficiently sensitive to detect BBB leakage, we assessed 10- and 70-kDa tracer leakage
166 before and after the establishment of BBB function (at 3 and 7 dpf[21]). With both 10- and 70-
167 kDa tracers, we could detect an open BBB at 3 dpf that was closed at 7 dpf (**Fig. 2e–f**).
168 Together, these results show that we can accurately measure BBB leakage and integrity in
169 zebrafish and that based on these measures neither pericytes nor vSMCs are necessary for
170 BBB function during larval stages.

171 To investigate how mural cells control cerebral vasculature at later stages of life, we tissue-
172 cleared brains of adult stage *pdgfrb* mutants and siblings[44] and performed whole brain imaging.
173 We confirmed loss of pericytes and vSMCs at this stage using *TgBAC(pdgfrb:EGFP)*^{uq15bh} and
174 *TgBAC(acta2:EGFP)*^{uq17bh} (**Fig. 3a–b**). We examined a consistent region of the left optic
175 tectum (midbrain) and detected decreased branching of capillaries and increased diameter of
176 major vessels (**Fig. 3d–f**). The observed vessel dilation was restricted to larger caliber arteries
177 that would normally be invested with vSMCs (**Extended Data Fig. 4a–b**) and was not seen in
178 capillaries in this region of the brain (**Fig. 3e–f**). The loss of vSMCs was observable from the
179 earliest stages of vSMC development and artery dilation was observed by 21 dpf, consistent
180 with previous studies[13] (**Fig. 3c**, **Extended Data Fig. 4c–d**). This suggests that major vessel

181 dilation seen in *pdgfrb* mutants is due to loss of vSMCs and that reduced branching of
182 capillaries is due to loss of pericytes (given the timing observed in **Fig. 1**).

183 To investigate BBB integrity at later stages, we injected 3-month-old adult zebrafish with 10-
184 kDa Dextran. Brightfield imaging of vibratome-sectioned brains revealed severe aneurysms
185 across large caliber vessels (**Fig. 4a**) with blood pooling that was potentially consistent with
186 vessel ruptures (**Fig. 4c**) as previously reported[35]. Furthermore, we detected parenchymal
187 accumulation of tracer dye closely associated with large caliber vessel aneurysms (**Fig. 4b–**
188 **c**). To quantify the distribution of parenchymal tracer dye from deep (around major artery
189 aneurysms) to superficial (capillary beds) brain regions, we measured fluorescence intensity
190 in 10 brain regions approximately 100 microns apart from medial to lateral locations. This
191 demonstrated accumulation of tracer dye in medial regions associated with aneurysm in
192 mutants (**Fig. 4d–e**). These animals showed little evidence of leakage in capillary beds, with
193 marginally higher tracer intensity in mutants than controls in lateral locations that could be due
194 to diffusion from medial locations with high concentrations of tracer (**Fig. 4e**). To better
195 understand this extravasated tracer accumulation, we conducted whole brain imaging after
196 tracer injection in 5-month-old adults. Interestingly, we observed highly localized 70-kDa tracer
197 accumulation in regions that could be considered leakage "hotspots" at large caliber vessel
198 aneurysms (**Fig. 5a**; **Supplementary Videos 1 and 2**).

199 As 10-kDa tracer showed higher sensitivity than 70-kDa tracer in our control experiments
200 (**Extended Data Fig. 2b–c**), we examined 10-kDa tracer injections at earlier stages and found
201 that hotspots were readily detectable from as early as 1 month using this lower molecular
202 weight tracer (**Fig. 5b**). The hotspots were not readily detectable using 70-kDa Dextran in 2-
203 month-old zebrafish, consistent with increased sensitivity of 10-kDa tracers (**Extended Data**
204 **Fig. 5a–d**). Interestingly, the quantification of hotspots in whole cleared brains at 1 and 5
205 months of age showed that the number increased with aging, suggesting a progressive loss
206 of BBB integrity at focal sites of leakage (**Fig. 5c**). To further understand the nature of leakage
207 hotspots, we examined red blood cells in *pdgfrb* loss-of-function adults. We used *pdgfrb*
208 Crispant knockouts, which we validated by finding that F0 CRISPR consistently reproduced
209 the adult mutant phenotype (**Extended Data Fig. 5e–f**). Using the *Tg(gata1:DsRed)*^{sd2}
210 transgenic line to label erythrocytes, together with tracer injection, we found that knockout
211 animals showed tracer accumulation concomitant with extravasated red blood cells at
212 hotspots (**Fig. 5d**). This identified hotspots as sites of focal hemorrhage. Notably, these sites
213 were not detected at capillaries (**Fig. 5e**). Taken together, this shows that as mutants age,

214 loss of BBB integrity is associated with an increasing number of hotspot sites of focal
215 hemorrhage, that are found along aneurysmal vessels.

216 The quantification of tracer dye intensity at 2 hpi in adult mutants from medial (major vessels)
217 to lateral (capillaries) locations indicated leakage most closely associated with hotspot focal
218 hemorrhages. However, the intensity of tracer dye found in the lateral capillary regions was
219 measurably higher than in control animals (**Fig. 4e**). To test if this was likely due to progressive
220 diffusion of tracers from medial to lateral locations or if there may be some local leakage at
221 capillaries, we examined 10-kDa tracer leakage at 0.5 and 6 hpi. While hotspots could be
222 detected at 0.5 hpi, we detected little tracer accumulation in medial locations and no evidence
223 of parenchymal tracer leakage at lateral capillary locations (**Fig. 5f, h**, **Extended Data Fig.**
224 **6a–a′′**). However, after 6 hours of diffusion of tracer within the brain, we clearly observed
225 tracer at both medial and lateral locations, with higher intensity in medial locations (**Fig. 5g**, **i**,
226 **Extended Data Fig. 6b–b′′**). While we cannot rule out the possibility of slow leakage of tracer
227 at capillaries occurring concurrently with leakage at hemorrhages, these observations seem
228 consistent with a primary source of leakage at focal hemorrhages, followed by diffusion of
229 tracer throughout the parenchyma.

230 Pericytes are proposed to regulate the BBB by suppressing transcytosis through brain
231 capillary ECs[5,6]. This model is built on the observation by electron microscopy of the induction
232 of increased numbers of vesicular structures and caveolae in leaky pericyte-deficient
233 vessels[5,6]. To investigate if the loss of BBB integrity is associated with ultrastructural changes,
234 we performed electron microscopy. We imaged large caliber vessels and capillaries (**Fig. 6a–**
235 **b**, **Extended Data Fig. 7a**) and examined cellular junctions, basement membrane and
236 caveolae (defined as uncoated vesicular profiles of <100 nm diameter). While tight junctions
237 between endothelial cells remained intact, caveolae numbers along large vessel aneurysms
238 in *pdgfrb* mutants were significantly increased (**Fig. 6a′′–c**). This increase was almost
239 exclusive to the abluminal side of the ECs (**Fig. 6c**)**.** This abluminal accumulation of caveolae
240 may be more associated with changes in the mechanical state of ECs (as caveolae are highly
241 regulated by membrane tension[45,46]) than changes in intracellular transport. Furthermore, we
242 detected thickening of basement membrane (BM) (**Fig. 6d**), gaps in the BM and fluid
243 accumulation outside the vessel wall at aneurysms in mutants. We found no obvious
244 difference in the caveolae density in capillary ECs of *pdgfrb* mutants compared with siblings
245 (**Extended Data Fig. 7b**). Thus, leakage hotspots at aneurysms are associated with a loss of
246 the normal flattened morphology of ECs, caveola induction and disruption of the BM, all factors
247 that could contribute to or be observed concurrent with vessel wall rupture.

248 **Discussion**

249 Brain vasculature is endowed with mural cells that control vascular development and
250 stability[3,4,13,47]. Studies in rodents have shown that pericytes regulate BBB integrity, with
251 knockout of *Pdgfb* or *Pdgfrb* leading to vessel dilations and brain hemorrhages from early in
252 development[3,4]. However, hypomorphic mutant alleles impacting *Pdgfb* or *Pdgfrb* show
253 increased leakage of the BBB, with the severity of the leakage phenotype correlating with the
254 expressivity of the pericyte phenotype[5,6]. BBB leakage is associated with increased vesicular
255 structures in ECs and the "open" BBB state in the absence of mural cells is thought to be
256 caused by hotspots of increased EC transcytosis[2,48]. Other potentially relevant pathways in
257 ECs that could be altered by pericytes include altered cell-cell adhesion (e.g. Cldn5[14]), control
258 of Mfsd2a[21,26], Netrin1-Unc5B signaling[49] or vitronectin regulation of integrin receptors[50], but
259 direct links are yet to be established. Some studies using other models to deplete pericytes in
260 mice have reported loss of pericytes without vessel leakage. For example, optical or chemical
261 ablation of pericytes in the brain or retina of mice can be achieved without compromising the
262 integrity of BBB or blood-retinal barrier[51,52], however these methods may induce inflammatory
263 or compensatory mechanisms that also influence local vasculature. Taken together, these
264 studies show that mural cells and in particular pericytes control the BBB in mammals, yet the
265 precise downstream mechanisms by which pericytes regulate EC function require further
266 study.

267 We show using zebrafish that mural cells are involved in cerebrovascular patterning in larval
268 and juvenile animals, but these vessels maintain BBB function in the absence of mural cells.
269 While the zebrafish BBB has been shown to be established between 3 and 5 dpf, we find that
270 our leakage assays at 7 and 14 dpf in mural cell-deficient *pdgfrb* mutants indicate intact BBB
271 function and wildtype vessel integrity. This is unlikely to be due to technical issues with
272 detecting leakage, as multiple measures and methods of tracer normalization produced
273 consistent results. Furthermore, we can readily detect the "open" BBB before it closes during
274 development (**Fig. 2e–f**). This demonstrates that a functional vertebrate BBB can exist in the
275 absence of pericytes. Importantly, while other species have a glial cell BBB (e.g. *Drosophila*,
276 some sharks and sturgeon), the zebrafish is well established to have an EC barrier and the
277 glial cell coverage at the stages analyzed here is far from complete[36], making glial cell
278 compensation for a loss of pericytes unlikely. There are other evolutionary differences (e.g.
279 developmental timing, innate immune differences[42,53]) between zebrafish and mammals and
280 our observation of intact BBB function without mural cells could represent an additional
281 divergence. However, the high level of conservation of developmental pathways in BBB ECs

282 and the very similar transcriptional signatures of both neurovascular ECs and mural cells
283 between species[19,30,34,54] may make this surprising. Once additional mechanisms of pericyte-
284 EC crosstalk are established in mice and zebrafish, deeper mechanistic comparative studies
285 will help to better understand if our observations identify major differences in BBB control
286 between these organisms or not.

287 Ultimately, in older mutants from 1 month of age onwards, BBB integrity defects are
288 observable with major arteries progressively harboring aneurysms and focal hemorrhages
289 (leakage hotspots). These aneurysms are likely due to the loss of vSMCs seen in our *pdgfrb*
290 mutants and other zebrafish *pdgfrb* mutant models[13,35]. Adult mutant hotspots show
291 extravascular erythrocytes and tracer dye, demonstrating that focal hemorrhages are a cause
292 of vessel leakage. Similar to this, in *Pdgfb* or *Pdgfrb* mutant mice with strong phenotypic
293 expressivity, hemorrhages are also reported (although not in mild or hypomorphic mutants
294 used in BBB studies)[3,4,12]. These observations suggest a highly conserved role for mural cells
295 in the regulation of aneurysm and hemorrhage in mice and zebrafish. In our zebrafish model,
296 BBB leakage in juvenile and adult animals appears to only be observed once hemorrhages or
297 hotspots are present. Coupled with the fact that larval zebrafish can have no mural cells, but
298 intact barrier function, we suggest that any roles for mural cells in BBB integrity beyond control
299 of aneurysm and hemorrhage are likely to be minor roles in this setting. It remains possible
300 that there is slow undetectable capillary leakage, but future models that specifically lack
301 capillary pericytes and not vSMCs will be needed to test this. Understanding the nature of
302 hotspot leakage more broadly in various mammalian and non-mammalian models of mural
303 cell deficiency would seem likely to uncover further insights into BBB regulation. Deeper
304 understanding of the fundamental biology of the BBB is still needed and will pave the way for
305 increasingly sophisticated efforts to target the BBB in disease in the future.

306 **Methods**

307 **Zebrafish husbandry**

308 Zebrafish work was conducted in compliance with animal ethics committees at the Peter
309 MacCallum Cancer Centre, The University of Melbourne and The University of Queensland.
310 The following previously published transgenic lines were used in this study:
311 *TgBAC(pdgfrb:EGFP)*^{uq15bh} [55], *Tg(kdrl:Hsa.HRAS-mCherry)*^{s916} [56], *Tg(kdrl:EGFP)*^{s843} [57],
312 *Tg(gata1:DsRed)*^{sd2} [58], *TgBAC(acta2:EGFP)*^{uq17bh} [55], and *Tg(5xUAS:RFP)*^{nkuasrfp1a} [59].

313 To ensure optical transparency, live imaging was performed in *slc45a2*
314 (ENSDARG00000002593) F0 knockout animals as previously described[60] or by adding
315 0.003% 1-phenyl-2-thiourea (PTU) to embryo water at 1-day post-fertilization (dpf).

316 **BAC recombineering and transgenesis**

317 The *TgBAC(abcc9:abcc9-T2A-mCherry)*^{uom139} transgenic line was generated by BAC
318 recombineering as previously described[61,62]. Briefly, T2A-mCherry insert with a kanamycin
319 cassette was amplified by PCR using *pCS2-T2A-mCherry-KanR* plasmid as template. The
320 primers used for amplifying the insert were:
321 5′-atggagcaggaggacggcctgtttgcatcttttgtcaaagccgacatgGAGGGCAGAGGAAGTCTGCTA-3′
322 5′-
323 aaaatggcttttattgatctgttaaggccaaaagtggtgtaaagtggggaTCAGAAGAACTCGTCAAGAAGGCG-
324 3′ (lowercase letters indicate homology arms to the BAC vector; uppercase letters indicate
325 primer binding sites on the template plasmid).

326 The amplified insert was introduced into *CH211-58C15* (*abcc9*) BAC clone containing a
327 pRedET plasmid (GeneBridge, Heidelberg, Germany) and iTol2 cassette. Approximately 1 nL
328 of purified BAC DNAs (100 ng/µL) mixed with *tol2* transposase mRNA (25 ng/µL) were injected
329 into single-cell stage embryos. Injected fish were raised to adulthood and screened by
330 fluorescence and PCR for germline transmission. The *pdgfrb:gal4FF* BAC construct was
331 generated previously[31] and was injected to produce the *TgBAC(pdgfrb:gal4FF)*^{um140} transgenic
332 line. The *pdgfrb:gal4FF* BAC construct was kindly provided by Dr. Nathan Lawson
333 (Department of Molecular, Cell, and Cancer Biology, University of Massachusetts Chan
334 Medical School, USA).

335 **Genome editing and genotyping**

336 The *pdgfrb*^{uq30bh} mutant strain was generated using CRISPR/Cas9-mediated genome editing.
337 The resulting allele carries a 39-bp deletion and a 5-bp insertion in exon 3 of *pdgfrb*
338 (ENSDARG00000100897), leading to a predicted frameshift and premature stop codon.

339 The gRNA sequence and genotyping primers used were:
340 gRNA binding site: 5′-GATGGTGACTAAGACGCGA-3′
341 Forward genotyping primer: 5′-CTTCCTTAGATCCTGACGTGTG-3′
342 Reverse genotyping primer: 5′-TATTGATGGGTTCGTCACCAG-3′

343 F0 *pdgfrb* crispants used were generated using Alt-R CRISPR-Cas9 reagents (IDT). The
344 gRNA sequence and genotyping primers used were:

345 Dr.Cas9.PDGFRB.1.AA: 5′-GATGGTGACTAAGACGCGAG-3′
346 Forward genotyping primer: 5′-CTTCCTTAGATCCTGACGTGTG-3′
347 Reverse genotyping primer: 5′-TATTGATGGGTTCGTCACCAG-3′
348 Dr.Cas9.PDGFRB.1.AB: 5′-CTCGGTGCACACATAAACCC-3′
349 Forward genotyping primer: 5′-GACGAGAACATCCCAGACTTTC 3′
350 Reverse genotyping primer: 5′-GCGTGTAAACAAATCCTAACGG-3′

351 Throughout this study, sibling control fish were pooled homozygous wild-type and
352 heterozygous animals, as no significant differences were detected between these genotypes
353 (e.g. **Extended Data Fig. 1c-d**).

354 **Fluorescent tracer injections**

355 Fluorescently conjugated tracers used were: 1 kDa NHS Ester–Alexa Fluor™ 405 (Thermo
356 Fisher: A30000), 10 kDa Dextran–Cascade Blue (Thermo Fisher: D1976), 10 kDa Dextran–
357 Alexa Fluor™ 647 (Thermo Fisher: D22914), 70 kDa Dextran–Fluorescein (Thermo Fisher:
358 D1822), 2000 kDa Dextran–Tetramethylrhodamine (Thermo Fisher: D7139) each at 5 mg/mL.

359 Larvae (3–7 dpf) were anesthetized with tricaine and embedded in 0.5% low-melting agarose
360 (Bio-Rad 1613112) in E3 water on 35-mm glass-bottom dishes (MatTek P35G-1.5-20-C).
361 Approximately 5 nl was injected into the posterior cardinal vein (PCV). At 14 dpf, tracers were
362 injected into the PCV with ~10 nL tracer on 3% agarose pads. In juveniles and adults retro-
363 orbital injections were performed[63] on 3% agarose pads, with 0.2 µL or 0.5 µL tracer
364 respectively. Tracers were injected individually or co-injected (1–70 kDa with 2000 kDa)
365 depending on experimental design.

366 **Imaging**

367 *Sample preparation*

368 For live imaging at 3-14 dpf, larvae were mounted in 0.5% low-melting point agarose in E3
369 embryo water on a 35-mm glass bottom dish as previously described[64]. For fixed tissue
370 imaging, zebrafish were euthanized with tricaine overdose (10 g/L), fixed (as whole or after
371 brain extraction) in 4% paraformaldehyde (PFA) at 4°C overnight and washed in PBS. Brains
372 were embedded in 7% low-melting agarose in PBS (Tissue-Tek cryomolds) and coronally
373 sectioned at 200 µm thickness using a vibrating microtome (Leica VT1000 S). Sections were
374 mounted in RapiClear 1.52 solution (SunJin Lab, RC152201) for 3 hours at room temperature
375 prior to imaging. Whole fish or brain samples were cleared using CUBIC clearing adapted from
376 a previously described protocol[44]. Briefly, samples were incubated in CUBIC-L solution at
377 37°C overnight after fixation, washed and incubated in PBS at 4°C overnight, then incubated

in CUBIC-R solution at room temperature overnight. Samples were embedded in 2% agarose in CUBIC-R on a 35-mm glass bottom dish for imaging.

Image acquisition

Imaging was performed using the following microscopes and objectives: Olympus FV-MPERS upright multiphoton, 25x water dipping 1.05 NA (**Fig. 1a-b**,**f**; **Extended Data Fig. 5e**), Olympus FV3000 confocal 10x air 0.4 NA (**Fig. 3a-a′**; **Fig. 4b-b′**,**c′**,**d-d′**; **Fig. 5a-a′**; **Extended Data Fig. 5f**) and 40x oil immersion 1.4 NA (**Fig. 5d-e**), Olympus/Evident FV4000 confocal 10x air 0.4 NA (**Extended Data Fig. 2d-e**; **Fig. 3b-b′**; **Extended Data Fig. 4b,d**; **Fig. 5b**,**f**,**g**; **Extended Data Fig. 6a-b′′**) and 30x silicone immersion 1.05 NA (**Extended Data Fig. 1b**; **Fig. 2a**,**c**,**e**; **Extended Data Fig. 2b**; **Fig. 3c**; **Extended Data Fig. 4a-a′′**,**b′**,**c-c′**; **Fig. 5b′**) Nikon TiE with Yokogawa CSU-W1 spinning disk, Andor Sona sCMOS camera, 10x air 0.45 NA (**Extended Data Fig. 5a**,**b**), 20x air 0.75 NA (**Extended Data Fig. 3c**; **Extended Data Fig. 5a′**) and 40x water immersion 1.15 NA (**Extended Data Fig. 3a**). For tracer leakage assays, live imaging was performed at 2 hours post-injection (hpi), with a maximum variation in timing of 15 minutes due to the sequential imaging. Fixed tissue samples were collected at 0.5 hpi (**Fig. 5f**, **Extended Data Fig. 6**), 2 hpi (**Extended Data Fig. 2d–e**, **Fig. 4b-d′**, **Fig. 5a–b′**,**d–e**, **Extended Data Fig. 5a–b**) or 6 hpi (**Fig. 5g**). Stereomicroscope images were acquired using an NSZ-606 Zoom Stereomicroscope with a Tucsen Photonics Co. camera using TCapture/IS Capture software.

Transmission electron microscopy

Brains were extracted from euthanized 5-month-old zebrafish, fixed in 2.5% glutaraldehyde for 1 hour at room temperature and washed in PBS. For sectioning, the brains were embedded in 7% low-melting point agarose in PBS in cryomolds (Tissue-Tek) and were sectioned coronally using a vibrating microtome (Leica VT1000 S) with 200 µm thickness. Tissue sections were processed as described previously[65]. Briefly, tissue sections were immersed consecutively in a series of aqueous solutions: 1.5% potassium ferricyanide and 2% osmium tetroxide, 1% thiocarbohydrazide, 2% osmium tetroxide, 2% uranyl acetate and 0.06% lead nitrate using a Pelco Biowave at 80W under vacuum for 3 min each. Vibratome sections then underwent serial dehydration in increasing concentrations of ethanol, before serial infiltration with increasing concentrations of Procure 812 resin. Ultrathin sections were obtained using a Leica UC64 ultramicrotome and imaged on a JEOL JEM-1011 at 80 kV.

409 **Image processing**

410 Images were processed using Fiji[66] or Imaris 10.1 (Bitplane). Fluorescent images are shown
411 as maximum intensity projections (MIP), unless otherwise indicated. Vascular tracing (**Fig. 1c**)
412 and masked head regions (**Extended Data Fig. 1b**) are presented as snapshots, and videos
413 highlighting the hotspot leakage sites were generated using Imaris 10.1 and annotated in
414 Adobe Premier Pro 2024. Schematics were prepared in Adobe Illustrator 2025, and
415 pseudocolor overlays on transmission electron microscopy images were generated in Adobe
416 Photoshop 2024.

417 **Quantification of phenotypes**

418 *Gross anatomy*

419 Prior to imaging and genotyping, fish body lengths were measured from the tip of the head to
420 the tail base. Body length datasets were compiled from multiple independent
421 experiments. Survival was quantified using separately housed *pdgfrb*^{uq30bh} mutants and
422 siblings to enable continuous tracking. Sibling and mutant groups were initially sorted based
423 on *pdgfrb:EGFP*-positive cells in the brain using *TgBAC(pdgfrb:EGFP)*^{uq15bh}, and were
424 genotyped by PCR at the endpoint for each animal. Cerebrovascular aneurysms in juvenile
425 *pdgfrb* mutants were qualitatively classified as mild or severe on the basis of aneurysm size
426 relative to sibling controls.

427 *Mural cell number, vessel length, diameter and branching points*

428 Mural cell number was quantified by counting *pdgfrb:EGFP*-positive cells
429 (*TgBAC(pdgfrb:EGFP)*^{uq15bh}) in the brain associated with blood vessels (*Tg(kdrl:Hsa.HRAS-*
430 *mCherry)*^{s916}) in 3D view using Imaris 10.1. Vessel length, diameter and branching points
431 were quantified in Imaris 10.1. At larval stages, the lumenized midbrain central arteries
432 (*Tg(kdrl:Hsa.HRAS-mCherry)*^{s916}) branching from the middle mesencephalic central arteries
433 (MMCtA) was traced using the Filament tool and the total filament length (µm) was plotted.
434 Branching points within the traced vasculature were counted manually in 3D view. For adults,
435 100-µm thick maximum intensity projections (MIP) were generated from whole brain imaging,
436 using the continuation of the left MMCtA as an anatomical landmark to define a consistent
437 region of interest. For diameter measurements, 10 capillary diameters were measured per
438 sample. Vessel anatomy was assigned using Isogai et al[67] as reference.

439 *Tracer intensity*

440 The quantification of tracer intensity was performed on genotype blinded image sets using
441 Imaris 10.1 (Bitplane) and Fiji[66] in 50-µm thick MIPs, generated starting from 50 µm below the

442 dorsal longitudinal vessel (DLV) to avoid including potential leakage from surface vessels. For
443 live imaging quantifications, two different methods were used to validating findings. In the first
444 method, the midbrain region was masked using the tracer accumulation in the skin as an outer
445 boundary and metencephalic vessels as the border with the hindbrain. Vasculature was then
446 masked and removed using *Tg(kdrl:EGFP)*^{s843} *or Tg(kdrl:Hsa.HRAS-mCherry)*^{s916}, and mean
447 intensity of extravasated tracer within the midbrain was measured. Relative leakage by
448 molecular weight in wild-type animals was assessed by normalizing extravasated midbrain
449 tracer intensity to intravascular tracer intensity. For comparisons between groups (siblings
450 versus *pdgfrb* mutants, or for wild-type at 3 versus 7 dpf), extravasated midbrain tracer
451 intensity was normalized to vascular reporter intensity (*kdrl:EGFP* or *kdrl:Hsa.HRAS-mCherry*).
452 In the second method, in experiments including 2000-kDa dextran as an injection control,
453 extravasated 70- or 10-kDa dextran intensity in midbrain parenchyma was calculated from the
454 average intensity in four defined parenchymal regions. These values were normalized to the
455 vascular intensity of 2000-kDa dextran, calculated from the average intensity in four regions
456 within the DLV lumen. As such, for each data point: intensity=parenchymal tracer (10 or 70
457 kDa) intensity/luminal 2000-kDa tracer intensity. For datasets assessing leakage between
458 siblings versus *pdgfrb* mutants at 7 and 14 dpf (**Fig. 2, Extended Data Fig. 3**), we assessed
459 the raw (non-normalized) tracer intensity in the parenchyma and compared these values to
460 normalized values. We found that both normalization strategies improved the analysis,
461 reducing variance and controlling for differences in tracer delivery and image variation
462 between animals.

463 For tracer intensity quantification in sectioned brains, 50-µm thick MIPs were generated.
464 Tracer intensity outside the vasculature was measured at ~70-µm intervals from medial to
465 lateral within a 0.7-mm region in juveniles, and at ~100-µm intervals within a 1-mm region in
466 adults, due to differences in brain size. For tracer intensity quantification in sectioned brains,
467 50-µm thick MIPs were generated and dextran intensity outside the vessels was measured at
468 approximately every 70 µm from medial to lateral direction within 0.7 mm in juveniles and at
469 every 100 µm within 1 mm in adults due to size difference. These measurements were
470 normalized to vascular reporter intensity (*kdrl:EGFP*). MMCtAs served as anatomical
471 landmarks to ensure consistent region selection.

472 *Hotspot leakage sites*

473 Hotspot leakage sites were identified as prominent focal accumulations of fluorescent tracer
474 adjacent to and outside the vasculature. Quantification was performed in 3D using Imaris 10.1.

TEM quantification

Imaged sections were quantified using Fiji[66]. Caveolae were defined as circular profiles of less than 100 nm in diameter and were scored as luminal or abluminal based on proximity to each surface membrane (within 500 nm of each surface or in a thin-walled vessel the caveolae closest to each surface). Basement membrane thickness was scored in six different locations per vessel that were selected at random.

Statistical analysis

Graphic representations and statistical analyses were performed using GraphPad Prism 10. Shapiro–Wilk test was applied to test normal distribution of the data. Two-tailed Student's t-tests were used for two-group comparisons with normal distribution, and Mann–Whitney U tests for non-normal data. One- or two-way ANOVA followed by Tukey's post hoc test was used for multiple group comparisons. $P<0.05$ was considered statistically significant.

Data availability

Source datasheet 1 contains the numerical data used to generate the figures.

Acknowledgments

This project was supported in part by funding from Bright focus (A2018807S), the Australian Research Council (ARC) (DP210102712) and The Brain Cancer Centre (founded by Carrie's Beanies for Brain Cancer). B.M.H was supported by a National Health and Medical Research Council Senior Research Fellowship (1155221) and Investigator grant (2033008). R.G.P was supported by an ARC Laureate Fellowship (FL210100107). We thank the Centre for Advanced Histology and Microscopy (RRID:SCR_025432) at the Peter MacCallum Cancer Centre and Microscopy Australia Research Facility at the Centre for Microscopy and Microanalysis at The University of Queensland. We thank Koji Ando and Nathan Lawson for providing constructs and protocols for BAC recombineering. We also thank Kelly Smith and Marcos Sande Melon for academic discussions and technical suggestions.

Author contributions

O.F.B performed, analyzed experiments and co-wrote manuscript. B.M.H, conceptualized experiments, analyzed data and co-wrote manuscript. A.U.G, S.D, W.W, S.P, M.C.R.G, Y.W.L, J.R, R.P, A.L and A.F performed and analyzed experiments.

Conflicts of interest

The authors declare no conflicts of interest.

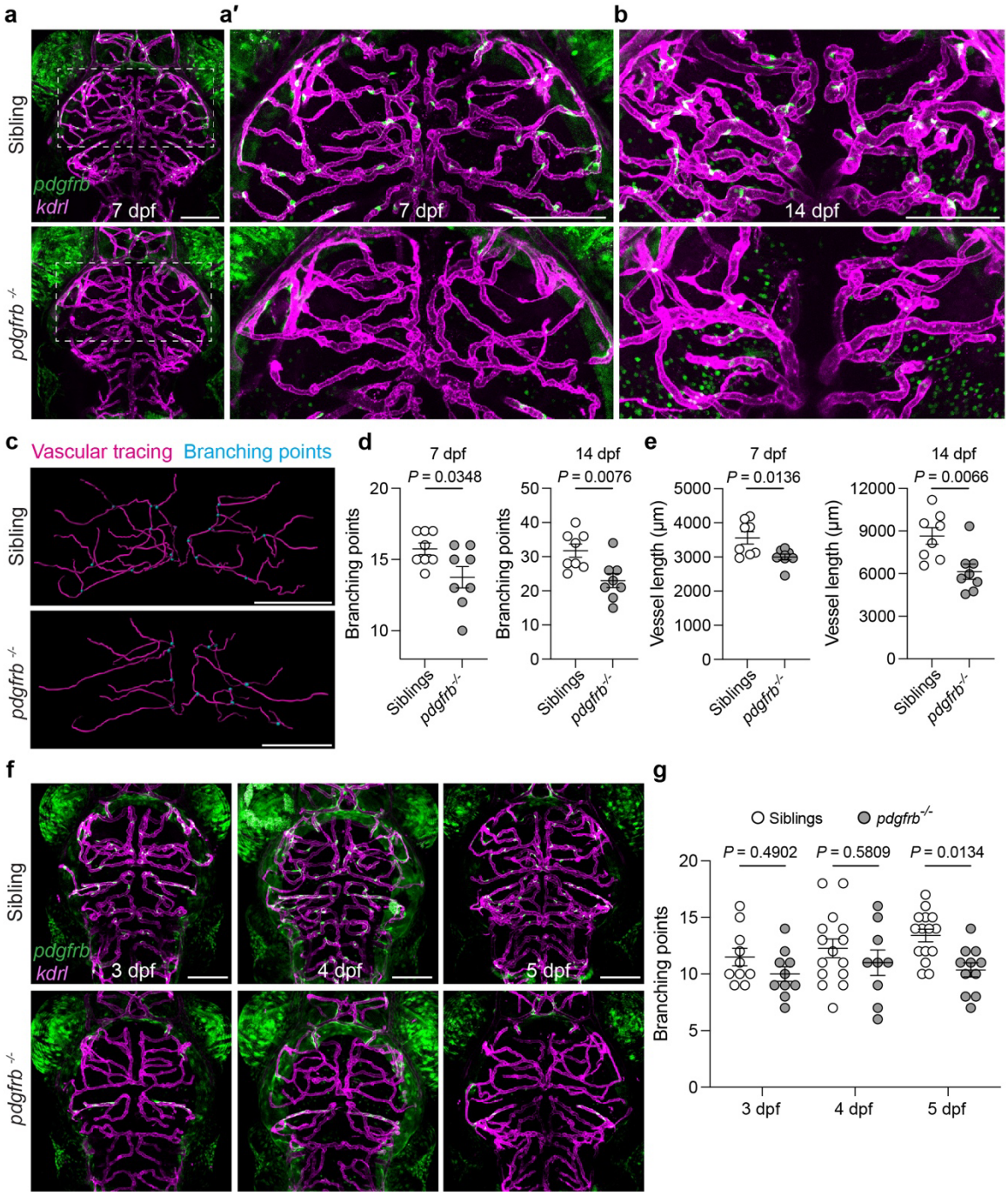

Fig. 1: Mural cell-deficient larval brain vasculature displays abnormal patterning.

a–b Maximum intensity projections of mural cells (*TgBAC(pdgfrb:EGFP)*^{uq15bh}) and brain vasculature (*Tg(kdrl:Hsa.HRAS-mCherry)*^{s916}) in siblings and *pdgfrb* mutants at 7 (**a**) and 14 dpf (**b**). (**a′**) shows enlarged view of the white box in (**a**) highlighting the midbrain central arteries.

c, Representative images of vascular tracing at 7 dpf using Imaris 10.1. Lumenized blood vessels branching from the middle mesencephalic central arteries in the midbrain were traced.

d–e, Quantification of midbrain branching points (**d**) and vessel length (**e**). Data are mean±SEM, n=8 per group, unpaired *t*-tests.

f, Maximum intensity projections of mural cells (*TgBAC(pdgfrb:EGFP)*^{uq15bh}) and brain vasculature (*Tg(kdrl:Hsa.HRAS-mCherry)*^{s916}) in siblings and *pdgfrb* mutants at 3-5 dpf.

g, Quantification of branching points of midbrain central arteries demonstrating the first detectable vessel patterning phenotype at 5 dpf. Data are mean±SEM, n=10 per group at 3 dpf, n=15 sibling and 9 *pdgfrb*$^{-/-}$ at 4 dpf, n=15 sibling and 11 *pdgfrb*$^{-/-}$ at 5 dpf, two-way analysis of variance (ANOVA) followed by multiple comparisons with Tukey's correction.

a, **a′**, **b**, **c**, **f**, Dorsal views, anterior up, scale bars: 100 µm.

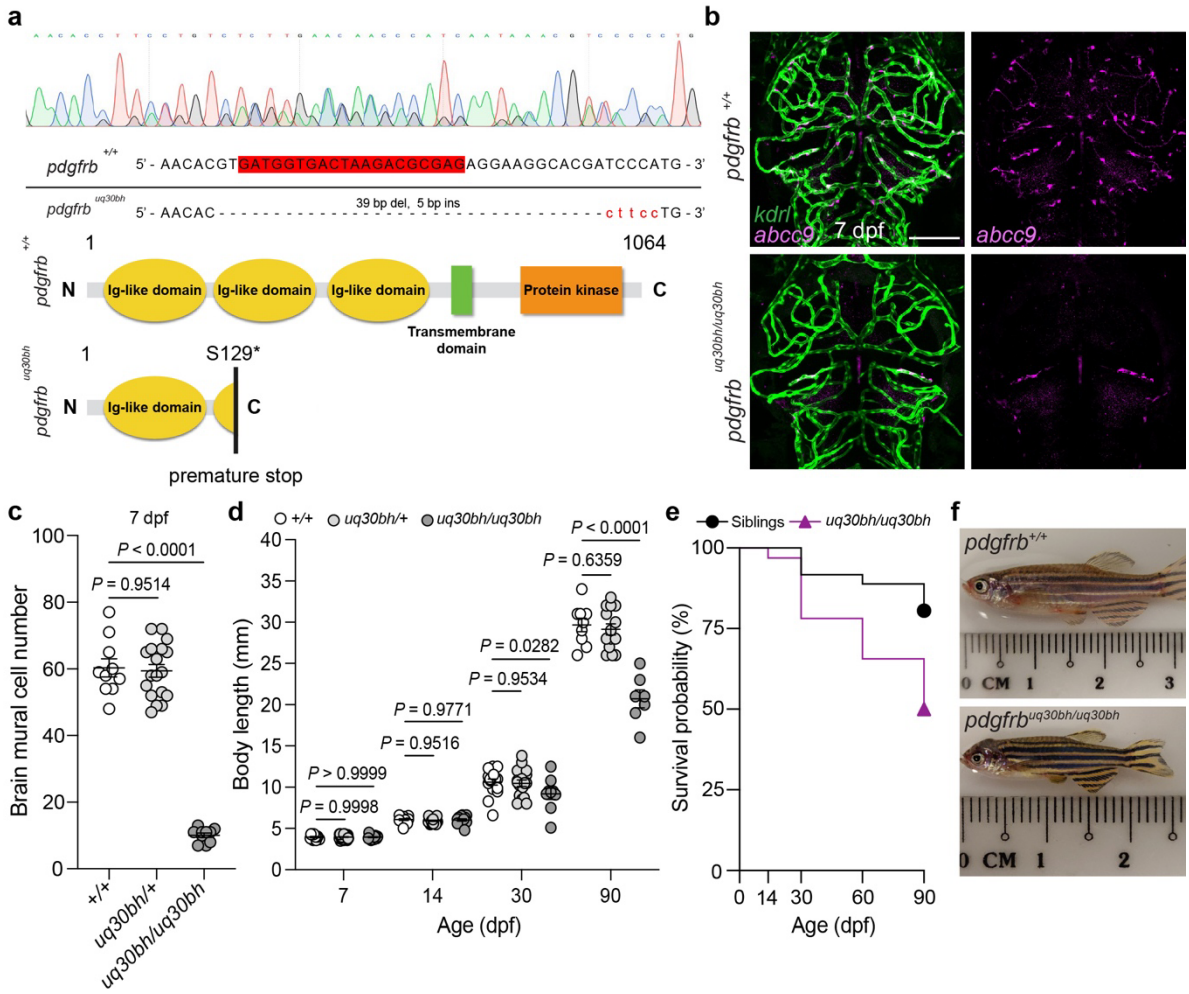
a
pdgfrb +/+ 5' - AACACGTGATGGTGACTAAGACGCGAGAGGAAGGCACGATCCCATG - 3'
pdgfrb uq30bh 5' - AACAC - - -

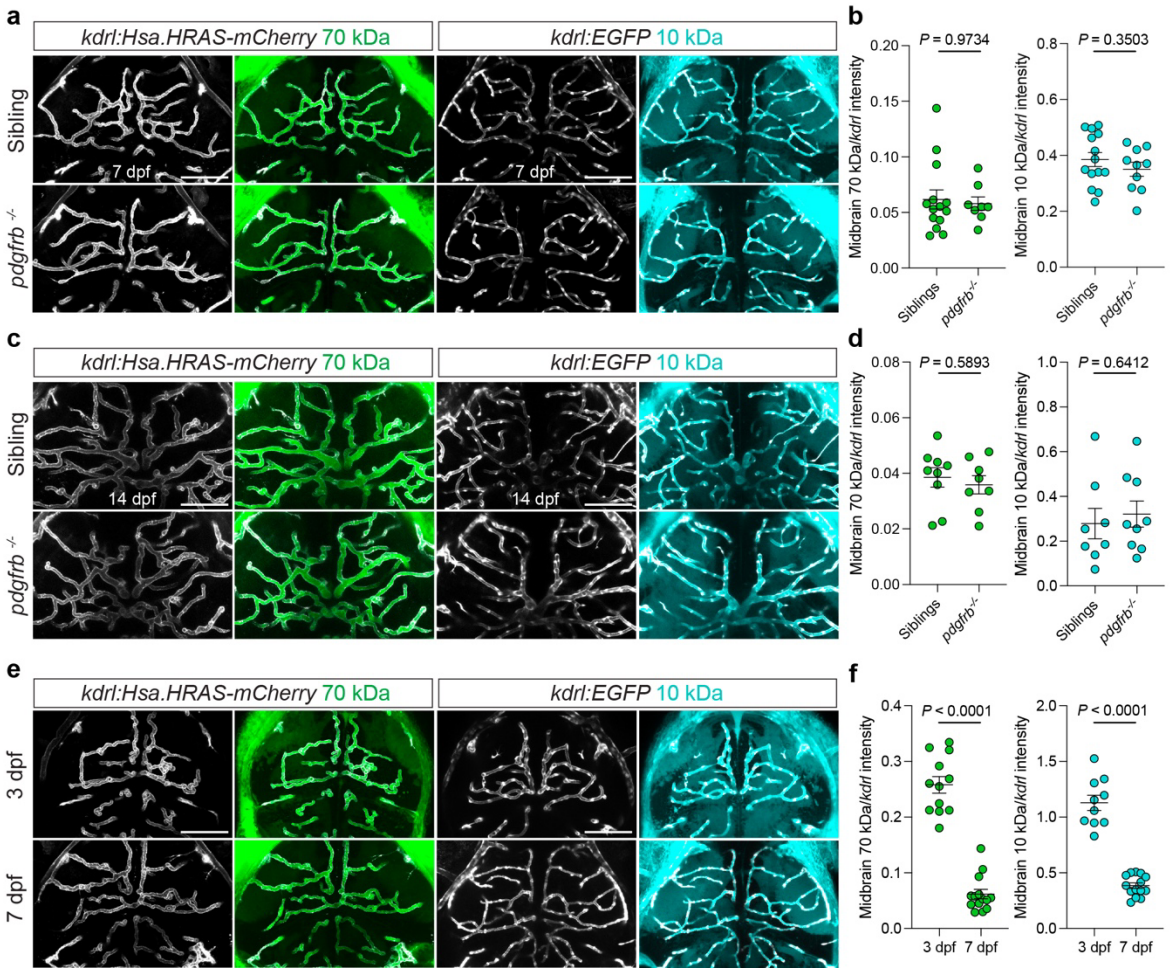

Fig. 2: BBB integrity is maintained in *pdgfrb* mutants during larval stages.

a, **c**, **e**, Fluorescent tracer leakage assays in the midbrain of zebrafish larvae using 70 kDa Dextran–Fluorescein or 10 kDa Dextran–Alexa Fluor™ 647, visualised with vascular reporters (gray) *Tg(kdrl:Hsa.HRAS-mCherry)*^{s916} and *Tg(kdrl:EGFP)*^{s843}. Siblings and *pdgfrb* mutants at 7 dpf (**a**) and 14 dpf (**c**) show no differences in tracer extravasation. Wild-type larvae at 3 and 7 dpf (**e**) serve as a positive control, illustrating reduced tracer leakage by 7 dpf. Dorsal views, anterior up, scale bars: 100 µm.

b, **d**, **f**, Quantification of midbrain parenchymal 70- and 10-kDa dextran fluorescence intensity normalized to vascular *kdrl* reporter intensity. Data are mean±SEM. At 7 dpf (**b**): n=14 siblings and 8 *pdgfrb*$^{-/-}$ for 70 kDa, and n=14 siblings and 10 *pdgfrb*$^{-/-}$ for 10 kDa. At 14 dpf (**d**): n=9 siblings and 8 *pdgfrb*$^{-/-}$ for 70 kDa, and n=8 siblings and 9 *pdgfrb*$^{-/-}$ for 10 kDa. For the positive control at 3 and 7 dpf (**f**): n=12 (3 dpf) and 14 (7 dpf) for 70 kDa, and n=10 (3 dpf) and 14 (7 dpf) for 10 kDa. Unpaired t-tests for 10 kDa dextran comparisons at 3 vs 7 dpf and for sibling vs *pdgfrb*$^{-/-}$ comparisons at 7 and 14 dpf, and for 70-kDa dextran at 14 dpf. Mann–Whitney U tests for 70-kDa dextran comparisons at 3 vs 7 dpf and for sibling vs *pdgfrb*$^{-/-}$ comparisons at 7 dpf due to non-normal data distribution.

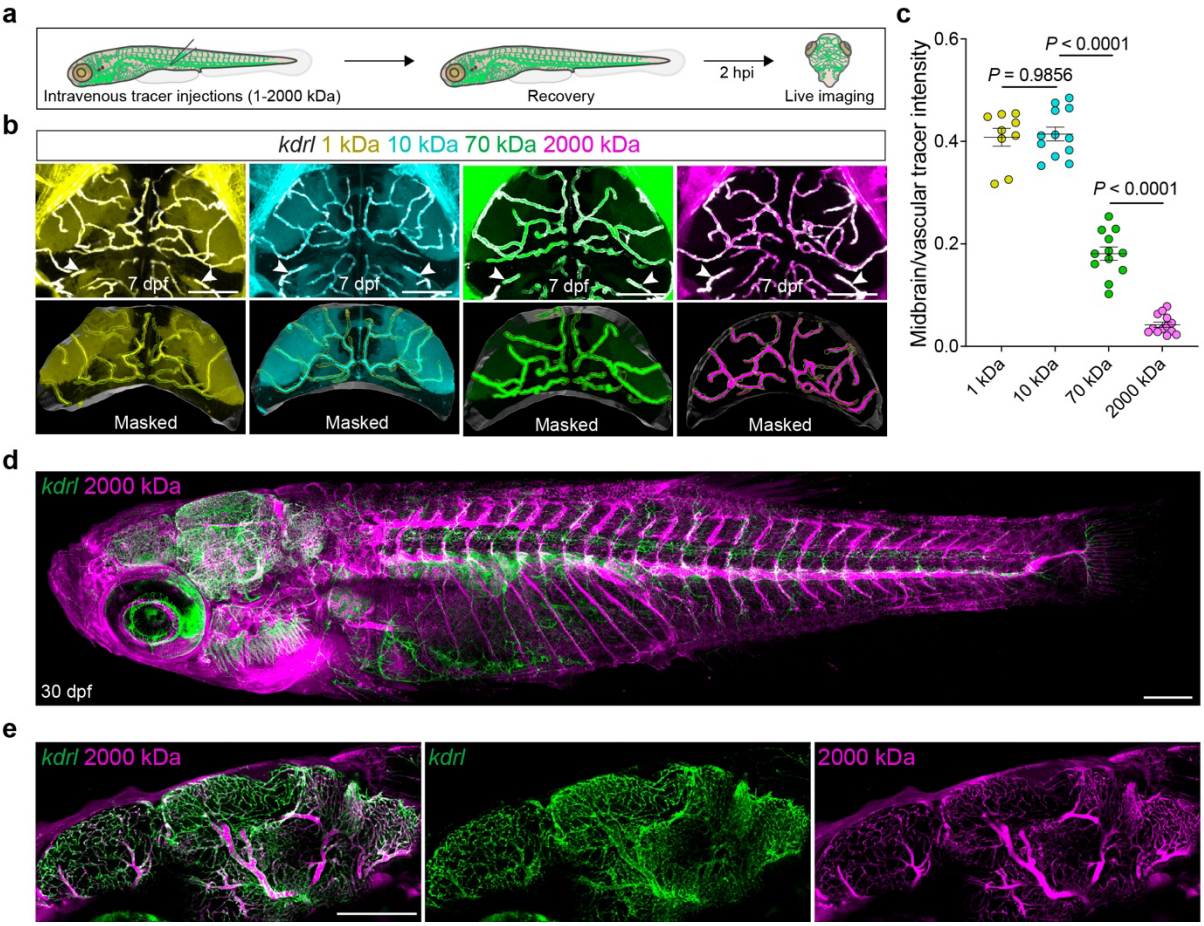

Extended Data Fig. 2: Controls for size-dependent tracer extravasation and distribution at larval and adult stages.

a, Schematic of fluorescent tracer leakage assay workflow in larvae. Tracers (1–2000 kDa) were intravenously injected, and fish were live imaged at ~2 hpi.

b, Confocal projections of tracer leakage assays in midbrain at 7 dpf, showing negative correlation between extravasation and tracer molecular weight. Larvae were imaged with *kdrl* reporter (gray) and intravenously injected 1 kDa NHS Ester–Alexa Fluor™ 405, 10 kDa Dextran–Alexa Fluor™ 647, 70 kDa Dextran–Fluorescein, or 2000 kDa Dextran–Tetramethylrhodamine. Masked regions show the quantified region in the midbrain. The vasculature was masked (yellow) with *Tg(kdrl:EGFP)*^{s843} in the 1-, 10- and 2000-kDa tracer injections and with *Tg(kdrl:Hsa.HRAS-mCherry)*^{s916} in the 70-kDa tracer injection. The midbrain was masked (gray) using the tracer accumulation in the skin for outer lining and using the metencephalic vessels (arrowheads) for posterior border. Dorsal views, anterior up, scale bars: 100 µm.

c, Quantification of midbrain parenchymal tracer fluorescence intensity normalized to vascular tracer fluorescence intensity. Data are mean±SEM, n=9 for 1 kDa, 12 for 10 kDa and 70 kDa, 13 for 2000 kDa, one-way ANOVA followed by multiple comparisons with Tukey's correction, $p<0.0001$ for all undisplayed pairwise comparisons.

d–**e**, Confocal projections of cleared juvenile zebrafish at 30 dpf showing retro-orbitally injected 2000 kDa Dextran–Tetramethylrhodamine diffusing across the vasculature. (**e**) shows a subset of z-slices from (**d**) focused on the mid-sagittal region of the brain, highlighting tracer distribution throughout the brain vasculature. Lateral view, anterior to left, scale bars: 500 µm.

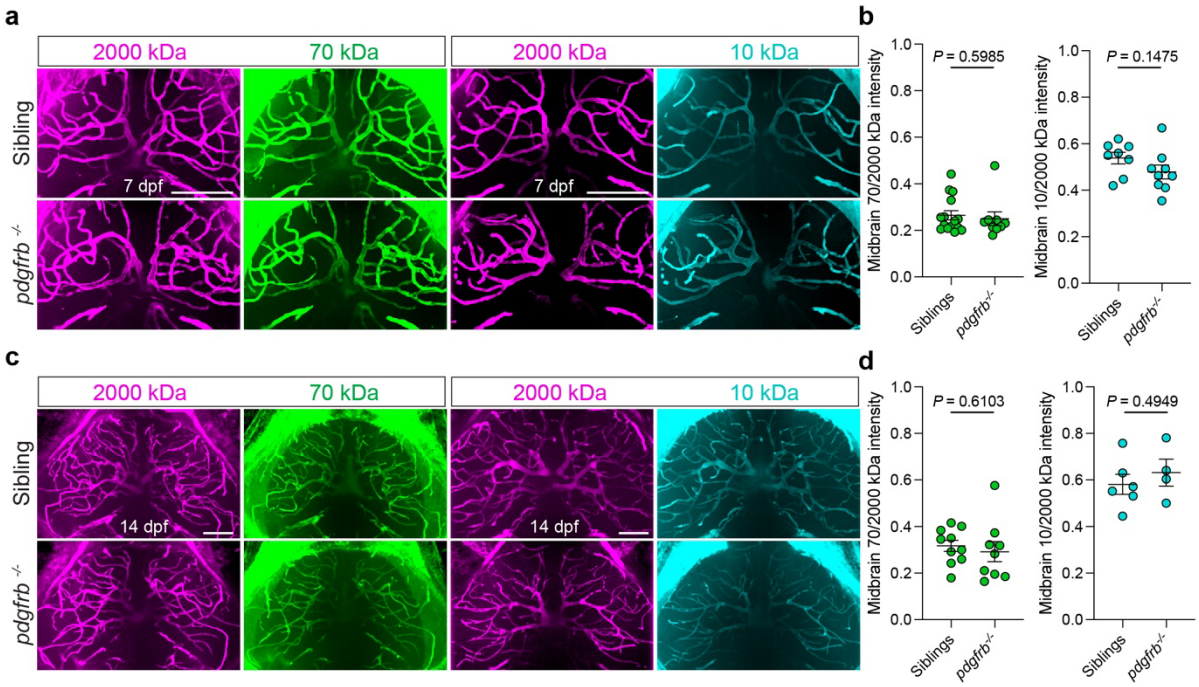

Extended Data Fig. 3: Tracer assays using an independent normalization method confirm that BBB integrity is maintained in *pdgfrb* mutant larvae.

a, **c**, Tracer leakage assays in the midbrain of zebrafish larvae in siblings and *pdgfrb* mutants at 7 dpf (**a**) and 14 dpf (**c**). 70 kDa Dextran–Fluorescein or 10 kDa Dextran–Cascade Blue was co-injected with 2000 kDa Dextran–Tetramethylrhodamine to detect parenchymal extravasation and injection volume. Dorsal views, anterior up, scale bars: 100 µm.

b, **d**, Quantification of midbrain parenchymal 70- and 10-kDa dextran fluorescence intensity normalized to vascular 2000-kDa dextran fluorescence intensity. Data are mean±SEM. At 7 dpf (**b**): n=15 siblings and 9 *pdgfrb*$^{-/-}$ for 70 kDa, and n=8 siblings and 9 *pdgfrb*$^{-/-}$ for 10 kDa. At 14 dpf (**d**): n=10 siblings and 9 *pdgfrb*$^{-/-}$ for 70 kDa, and n=6 siblings and 4 *pdgfrb*$^{-/-}$ for 10 kDa. Unpaired t-tests for 10 kDa at 7 and 14 dpf, 70 kDa at 14 dpf. Mann–Whitney U test for 70 kDa at 7 dpf due to non-normal distribution.

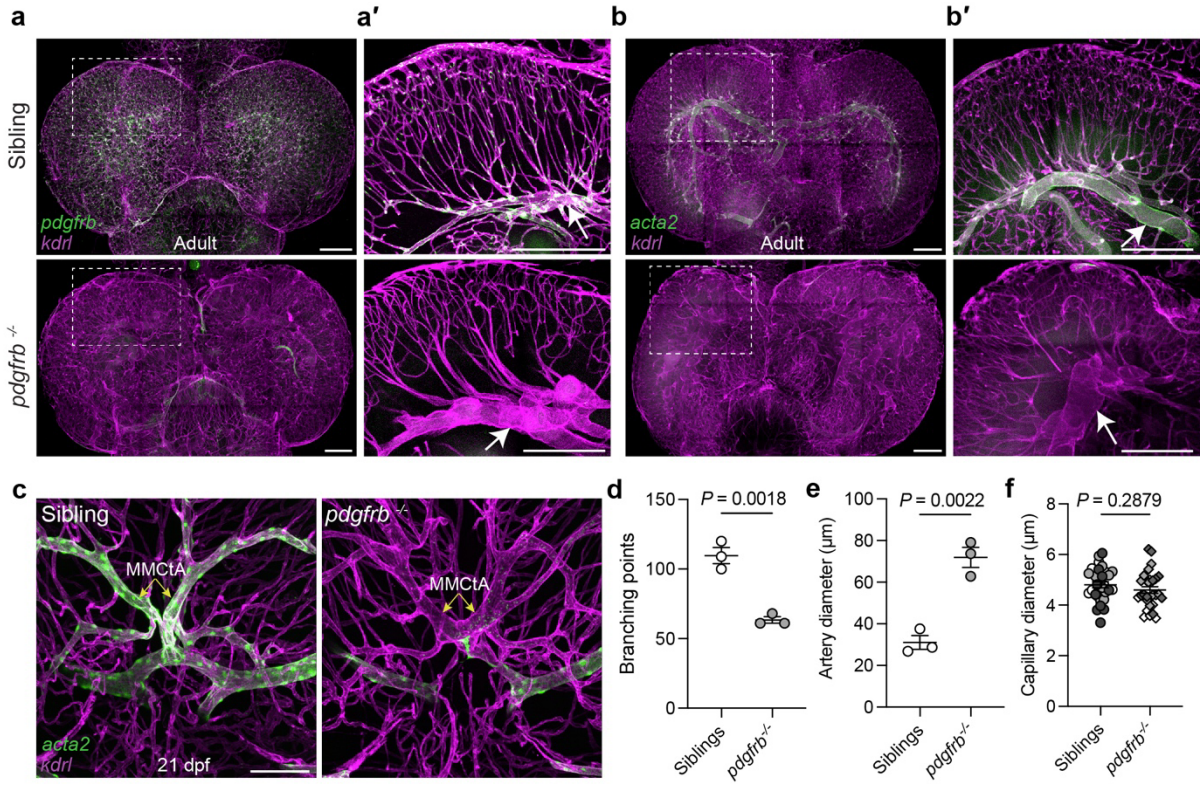

Fig. 3: Adult *pdgfrb* mutants lack mural cells and display dilated arteries.

a, **b**, Confocal projections of whole brain imaging in siblings and *pdgfrb* mutants at 5 months of age, showing brain vasculature using *Tg(kdrl:Hsa.HRAS-mCherry)*^{s916} and mural cells using *TgBAC(pdgfrb:EGFP)*^{uq15bh} (**a**) as a global marker and *TgBAC(acta2:EGFP)*^{uq17bh} (**b**) as a vSMC marker. Dorsal views, anterior up, scale bars: 250 µm.

a′, **b′**, Subset of z-slices from the whole brain imaging in (**a**) and (**b**) (white boxes) indicating mural cell loss and abnormal capillary network patterning. 100-µm-thick maximum intensity projections (MIP) were generated using the continuation of the left middle mesencephalic central artery (MMCtA, arrow) as an anatomical landmark. Scale bars: 250 µm.

c, Confocal projections from whole brain imaging in sibling and *pdgfrb* mutants at 21 dpf. Siblings show *acta2:EGFP*-positive vSMC coverage along MMCtAs (yellow arrows). *pdgfrb* mutants have dilated MMCtAs with absent vSMCs. Scale bar: 100 µm.

d–f, Quantification of capillary branching points (**d**), artery diameter (**e**) and capillary diameter (**f**) using the area shown in (**a′**). Data are mean±SEM, n=3 animals per group. Artery diameter was quantified by averaging 5 points per animal, and capillary diameter was quantified by measuring 10 capillary diameter per animal. Each animal marked with a different color in **f**. Unpaired t-tests for branching points and artery diameter, nested t-test for capillary diameter.

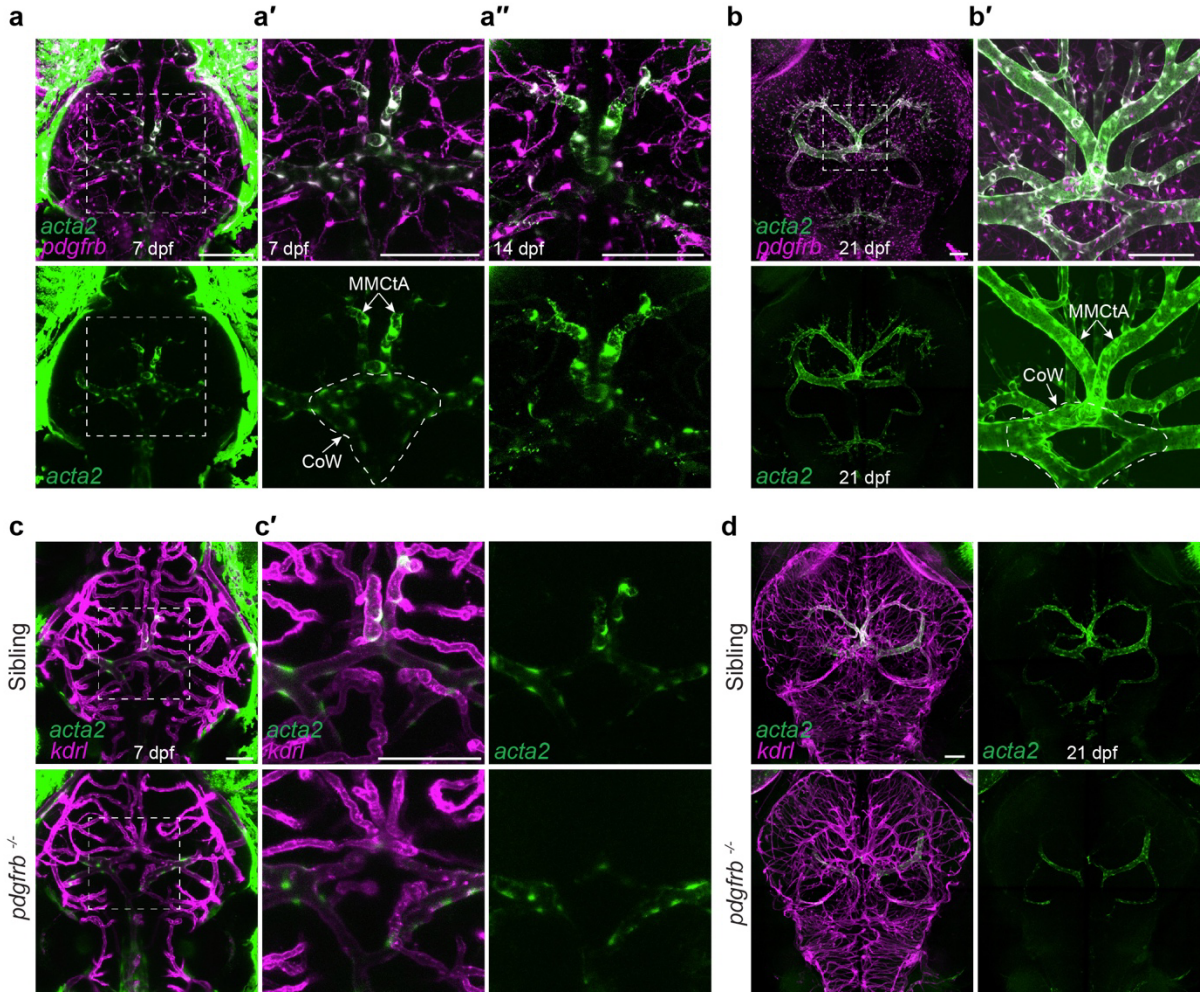

Extended Data Fig. 4: Development of *acta2:EGFP*-positive vSMCs in brain vasculature of siblings and *pdgfrb* mutants.

a–b′, Confocal projections of mural cells using *TgBAC(pdgfrb:gal4FF)*^{um140}; *Tg(5xUAS:RFP)*^{nkuasrfp1a} and *TgBAC(acta2:EGFP)*^{uq17bh}, live imaged at 7 and 14 dpf (**a–a′**) or imaged at 21 dpf post-fixation and clearing (**b–b′**).*acta2:EGFP* colocalizes with *RFP* driven by *pdgfrb:gal4FF* along MMCtAs (arrows) and at the Circle of Willis (CoW) (dashed line) by 7 dpf, expanding to arterioles by 21 dpf but absent from capillaries. (**a′**) and (**b′**) are enlarged views of white boxes in (**a**) and (**b**), respectively. (**a′′**) shows the same fish reimaged at 14 dpf.

c–d′, Confocal projections of developing smooth muscle cells (*TgBAC(acta2:EGFP)*^{uq17bh}) and brain vasculature (*Tg(kdrl:Hsa.HRAS-mCherry)*^{s916}) in siblings and *pdgfrb* mutants live imaged at 7 dpf (**c–c′**) or imaged at 21 dpf post-fixation and clearing (**d**). White boxes are magnified in (**c′**).

a–d, Dorsal views, anterior up, scale bars: 100 µm (**a–b′**, **d**), 50 µm (**c–c′**).

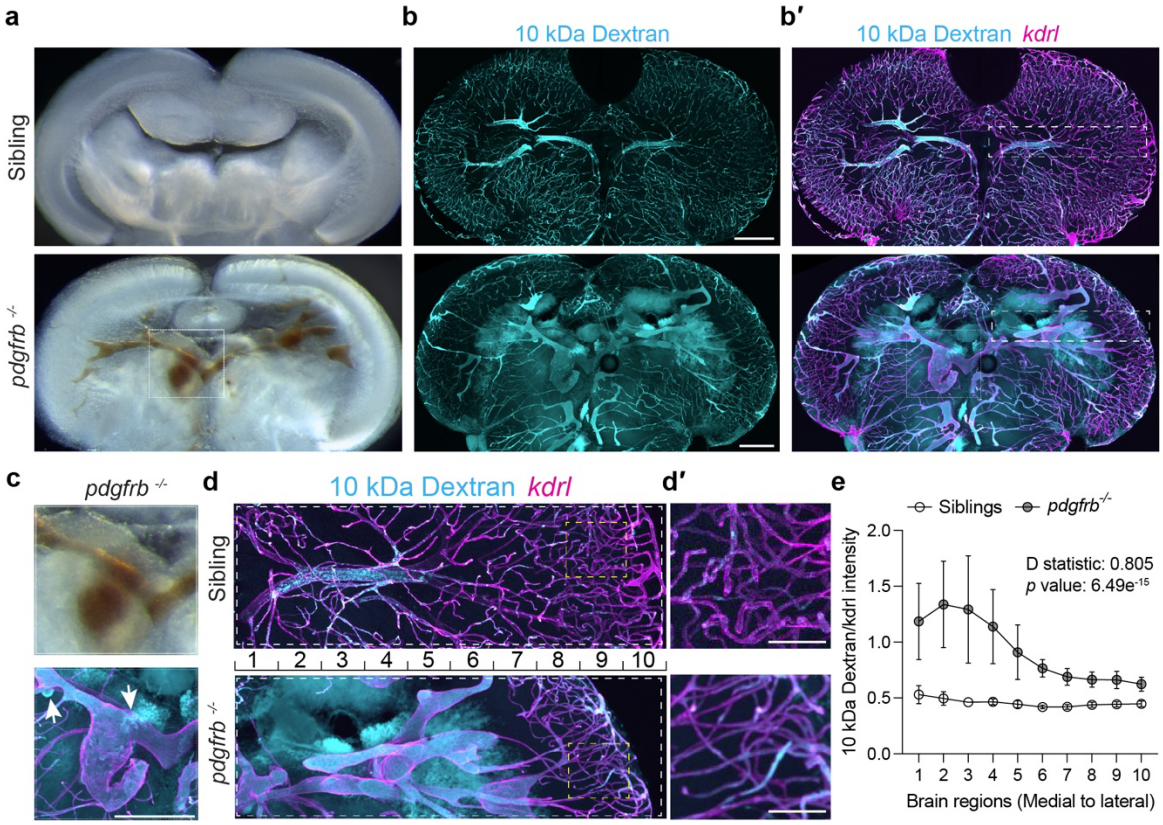

Fig. 4: Adult *pdgfrb* mutants display aneurysms and vascular integrity defects.

a, Representative images of coronal midbrain sections obtained from 3-month-old sibling and *pdgfrb* mutants.

b, Fluorescent tracer leakage assays in 3-month-old siblings and *pdgfrb* mutants (2 hpi). 10 kDa Dextran–Cascade Blue (**b**) was used to assess extravasation, and *Tg(kdrl:Hsa.HRAS-mCherry)*^{s916} was used to label the brain vasculature (merge in **b′**). Scale bar: 250 µm.

c–c′, Enlarged regions from (**a**) and (**b′**) (dotted box) displaying blood and tracer accumulation (arrows) in *pdgfrb* mutants. Scale bar: 250 µm.

d, Enlarged regions from (**b**) (dashed box) displaying vasculature and tracer leakage from medial (arterial region) to lateral (capillary region) regions. Area was divided into 10 regions (~100 µm intervals) for quantification.

d′, Enlarged view of yellow box in (**d**) showing capillary beds with intravascular tracer.Scale bar: 50 µm.

e, Quantification of parenchymal 10 kDa tracer intensity (medial to lateral) normalized to vascular *kdrl* intensity. Data are mean±SEM, each point represents average normalized tracer intensity per brain region, n=5 sibling and 4 *pdgfrb*$^{-/-}$, two-sample Kolmogorov–Smirnov test.

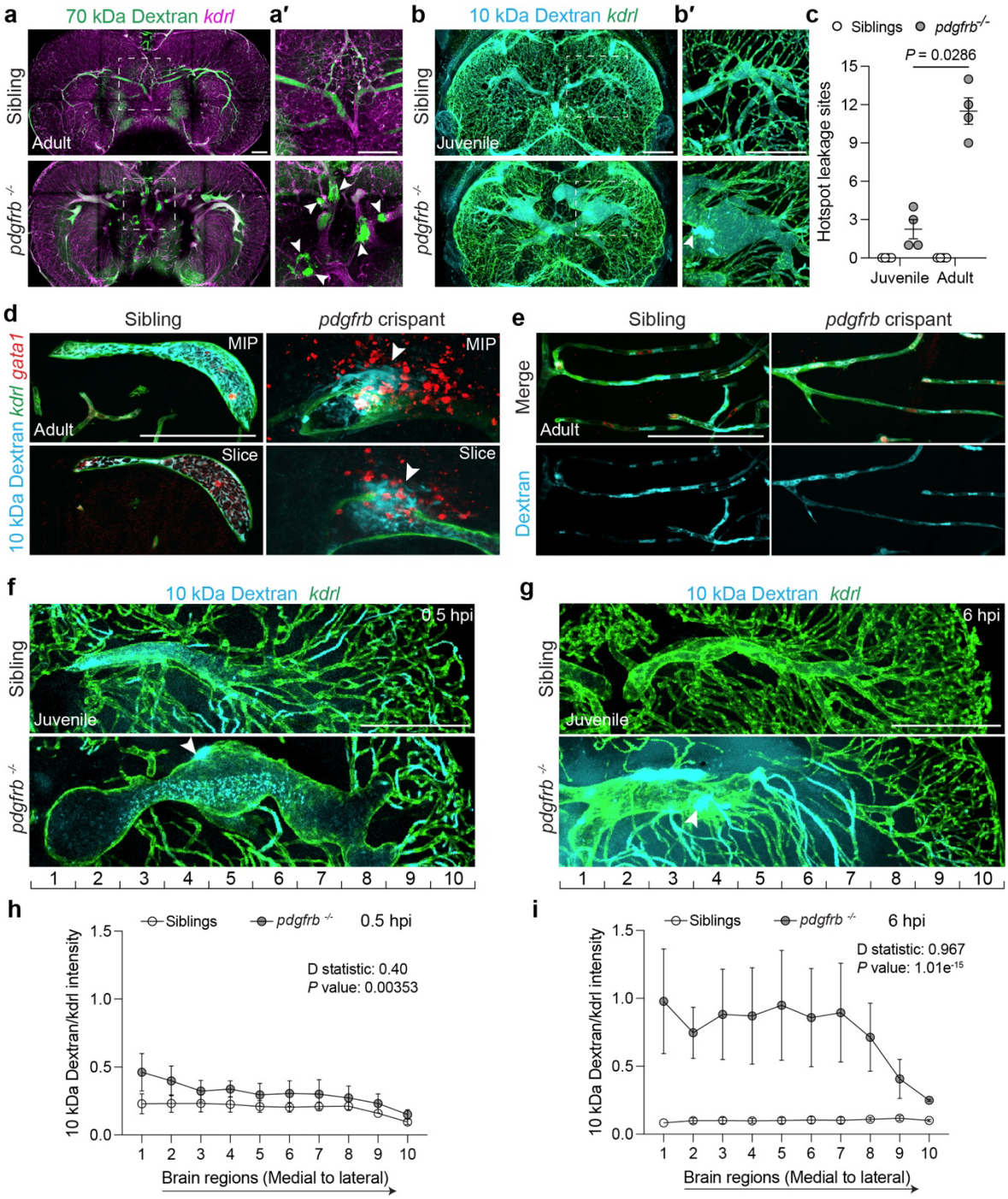

Fig. 5: Adult and juvenile *pdgfrb* mutants display vessel rupture and tracer accumulation at aneurysm hotspots.

a–a′, Fluorescent tracer leakage assays in 5-month-old sibling and *pdgfrb* mutants. 70 kDa Dextran–Fluorescein was detected outside the vessels marked by *Tg(kdrl:Hsa.HRAS-mCherry)*^{s916} at aneurysm hotspots (arrowheads) shown in white box (magnified in **a′**).

b–b′, Fluorescent tracer leakage assays in 1-month-old sibling and *pdgfrb* mutants. 10 kDa Dextran–Alexa Fluor™ 647 was detected outside the vessels marked by *Tg(kdrl:EGFP)*^{s843} at aneurysm hotspots (arrowhead) shown in white box (magnified in (**b′**)).

a–b, Brains were collected at 2 hpi, dorsal views, anterior is up, scale bars: 200 µm.

c, Quantification of hotspot leakage sites per animal in the midbrain region showing increased numbers in older animals. Data are mean±SEM, n=4 per group, unpaired t-test.

d–e, High resolution imaging of artery (**d**) and capillary zones (**e**) in brain regions of 10-week-old adult *pdgfrb* crispants and uninjected siblings after tracer injection (2 hpi). 10 kDa Dextran–Alexa Fluor™ 647 injected, blood vessels (*Tg(kdrl:EGFP)*^{s843}) and red blood cells (*Tg(gata1:DsRed)*^{sd2}) are shown in MIPs and single Z-sections. Arrowheads indicate examples of hotspots. Capillary zones shown in MIPs (all channels) and single 10-kDa Dextran channel lack hotspots. Scale bar: 100 µm.

f–g, Fluorescent tracer leakage assays in 1-month-old sibling and *pdgfrb* mutants shown in confocal projections of coronal midbrain sections collected at 0.5 hpi (**f**) or 6 hpi (**g**). 10 kDa Dextran–Alexa Fluor™ 647 was used to assess extravasation, and *Tg(kdrl:EGFP)*^{s843} was used to label the brain vasculature. The area was divided into 10 regions (~70 µm intervals) for quantification (see **Extended Data Fig. 6** for full section image). Arrowheads indicate examples of hotspots. Scale bar: 200 µm.

h–i, Quantification of parenchymal 10-kDa dextran intensity (medial to lateral) normalized to vascular *kdrl* intensity. Data are mean±SEM, each point represents average normalized tracer intensity per brain region, n=3 sibling and 5 *pdgfrb*$^{-/-}$ for 0.5 hpi, and n=3 per group for 6 hpi, two-sample Kolmogorov–Smirnov test.

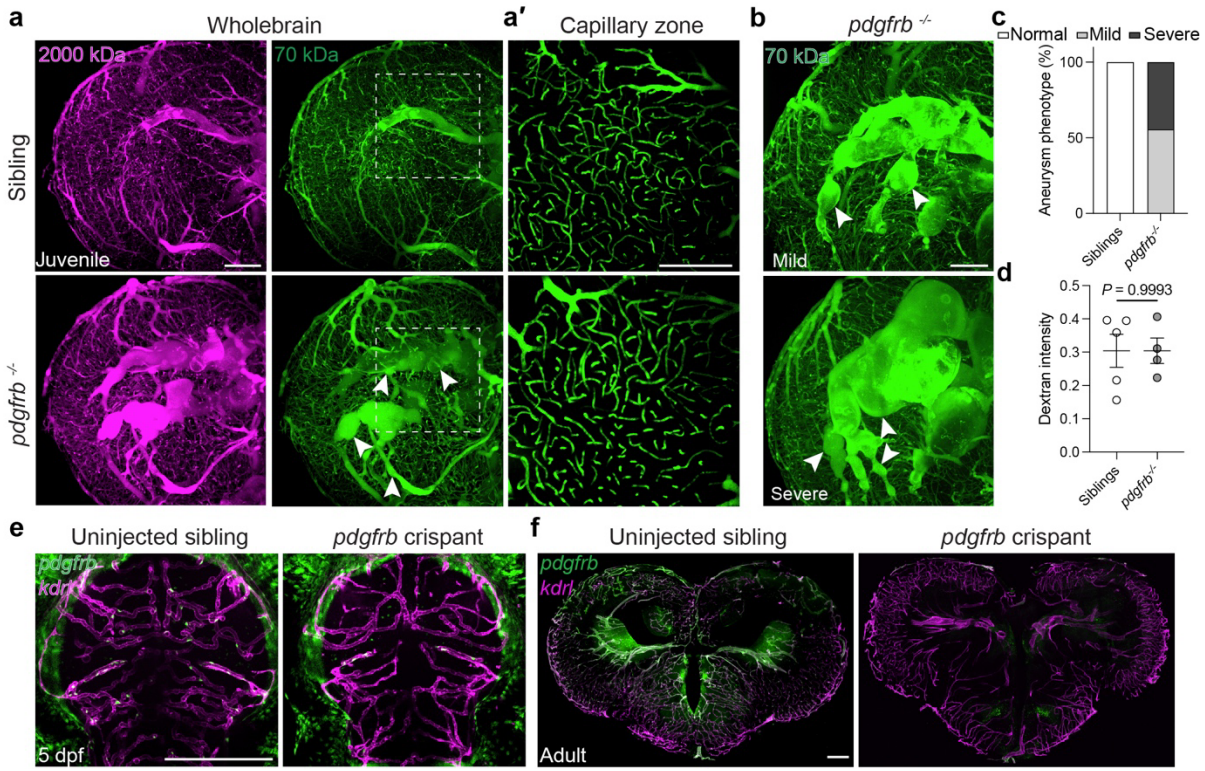

Extended Data Fig. 5: Arterial aneurysms in juvenile *pdgfrb* mutants and additional control data.

a, Fluorescent tracer leakage assays in 2-month-old zebrafish midbrain (2 hpi). 70 kDa Dextran–Fluorescein and 2000 kDa Dextran–Tetramethylrhodamine were co-injected to detect parenchymal extravasation and vascular tracer, respectively. Arrowheads mark aneurysms.

a′, Same brains reimaged at higher resolution targeting capillary regions. 30-µm-thick MIPs were displayed, starting 30 µm below the most superficial point of left hemisphere to exclude potential leakage from meningeal vessels.

b, Examples of mild and severe aneurysms (arrowheads) in *pdgfrb* mutants.

c, Quantification of the severity of aneurysms in sibling and *pdgfrb* mutants. Aneurysm phenotypes were qualitatively categorised based on severity; normal, mild and severe, n=11 per group.

d, Quantification of parenchymal 70-kDa Dextran intensity normalized to vascular 2000 kDa Dextran intensity using the data in (**a′**). Data are mean±SEM, n=5 sibling and 4 *pdgfrb*$^{-/-}$, unpaired t-test.

e–f, Validation that crispants phenocopy *pdgfrb* mutants (supporting data in **Fig. 5d–e**). Maximum intensity projections of mural cells (*TgBAC(pdgfrb:EGFP)*^{uq15bh}) and brain vasculature (*Tg(kdrl:Hsa.HRAS-mCherry)*^{s916}) in uninjected sibling and *pdgfrb* crispants at larva (5 dpf) and adult (10-week-old) stage. *pdgfrb* crispants lack brain mural cells and show dilated arteries in adulthood, phenocopying *pdgfrb*^{uq30bh} mutants.

a–b, **e**, Dorsal views, anterior up.

a–b, **e–f**, Scale bars: 200 µm.

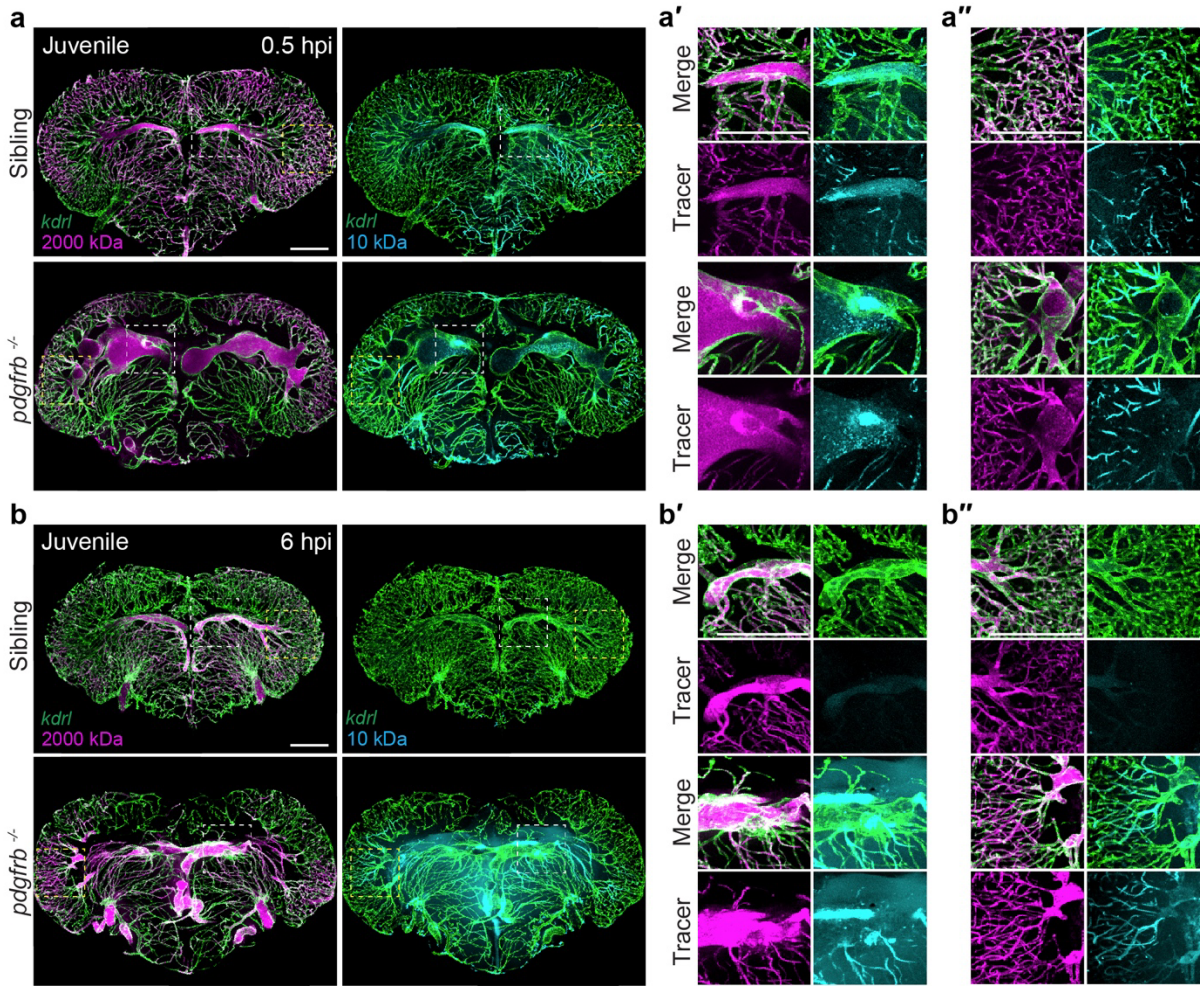

Extended Data Fig. 6: Coronal midbrain sections corresponding to Fig. 5f-g.

a, **b**, Entire coronal midbrain sections from tracer leakage assays in 1-month-old sibling and *pdgfrb* mutants shown as confocal projections. Brains were collected after retro-orbital co-injection of 10 kDa Dextran–Alexa Fluor™ 647 and 2000 kDa Dextran–Tetramethylrhodamine at 0.5 hpi (**a**) or 6 hpi (**b**), and *Tg(kdrl:EGFP)*^{s843} was used to label vasculature.

a′–a′′, **b′–b′′**, Enlarged views of regions indicated in (**a**) and (**b**). Panels (**a′**) and (**b′**) show medial regions (white boxes), whereas (**a′′**) and (**b′′**) show lateral regions (yellow boxes) in midbrain. Perfusion of tracer dyes and leakage hotspots are readily identifiable.

Scale bars: 200 µm.

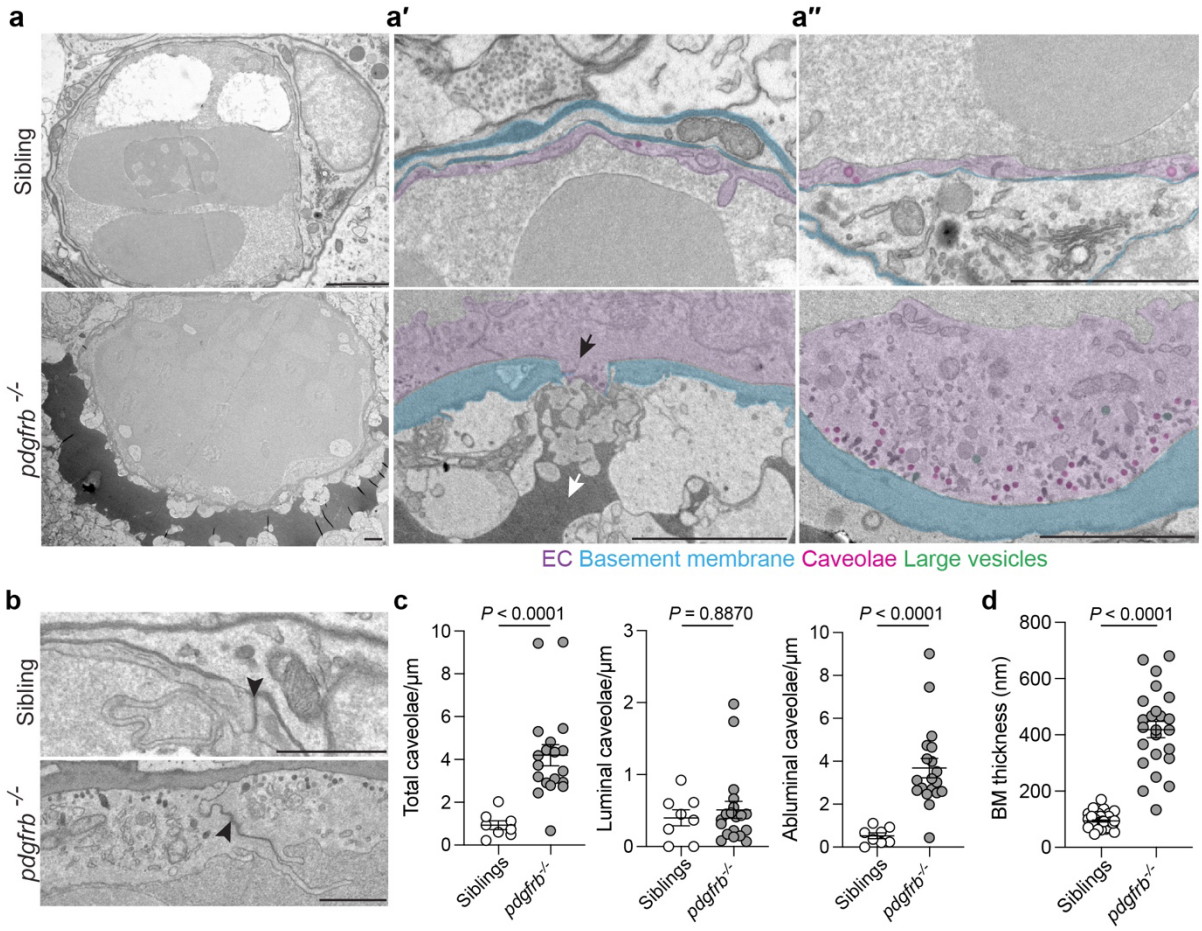

Fig. 6: Adult *pdgfrb* mutants display structural endothelial cell defects and vessel rupture.
a–a′′, Transmission electron microscopy images of sectioned adult zebrafish brain vessels at 5 months of age. *pdgfrb* mutants show basement membrane thickening and breakdown (black arrow), serum accumulation outside the vessels (white arrow) (**a′**), increased abluminal endothelial caveolae (**a′′**). Pseudocolors shown are ECs (purple), basement membrane (cyan), caveolae (magenta) and vesicles larger than 100 nm (green). Scale bars: 2 µm.
b, Magnified regions from (**a**) showing intact tight junctions (arrowheads) in both siblings and *pdgfrb* mutants. Scale bars: 1 µm.
c, Quantification of endothelial caveolae. Caveolae were defined as uncoated spherical profiles <100 nm in diameter and scored as luminal or abluminal (see methods for details). Measurements were made for n=3 vessels for each group and a total of 8 different cellular regions measured for siblings and 19 for mutants. Data are mean±SEM and are not distributed normally, Mann–Whitney U test was applied.
d, Quantification of basement membrane thickness, which was scored in 6 different regions per vessel with n=8 vessels in siblings 4 in *pdgfrb* mutants across n=3 animal per group. Data are mean±SEM, unpaired t-test. Data are mean±SEM and are not distributed normally, Mann–Whitney U test was applied.

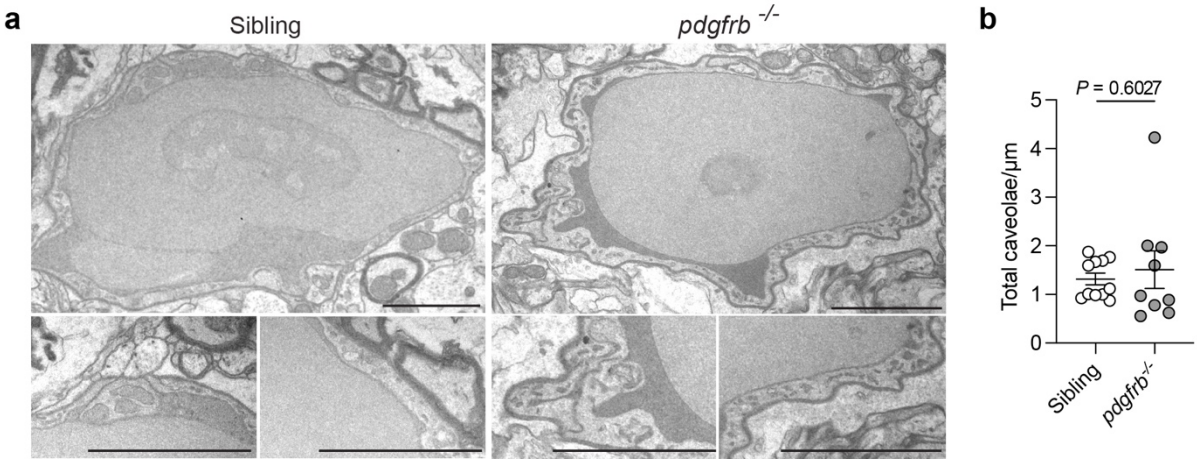

Extended Data Fig. 7: Adult *pdgfrb* mutants maintain normal endothelial ultrastructure in capillaries.

a, Transmission electron microscopy images of sectioned adult zebrafish brain vessels.

b, Quantification of endothelial caveolae in capillaries of siblings and *pdgfrb* mutants. Measurements were made for n=11 vessels in siblings and 9 in *pdgfrb* mutants across n=3 animals per group. Data are mean±SEM and are not distributed normally, Mann–Whitney U test was applied. No consistent defects were observed in capillaries.

Scale bars: 1 µm**.**

Source datasheet 1: Numerical data used to generate all plots presented in the figures

Source data in an excel spreadsheet in which each separate tab provides the individual measurements and numbers used to generate the plots presented in each figure.

References

1 Zhao, Z., Nelson, A. R., Betsholtz, C. & Zlokovic, B. V. Establishment and Dysfunction of the Blood-Brain Barrier. *Cell* **163**, 1064-1078 (2015). https://doi.org/10.1016/j.cell.2015.10.067

2 Armulik, A., Genove, G. & Betsholtz, C. Pericytes: developmental, physiological, and pathological perspectives, problems, and promises. *Dev Cell* **21**, 193-215 (2011). https://doi.org/10.1016/j.devcel.2011.07.001

3 Leveen, P. *et al.* Mice deficient for PDGF B show renal, cardiovascular, and hematological abnormalities. *Genes Dev* **8**, 1875-1887 (1994). https://doi.org/10.1101/gad.8.16.1875

4 Lindahl, P., Johansson, B. R., Leveen, P. & Betsholtz, C. Pericyte loss and microaneurysm formation in PDGF-B-deficient mice. *Science* **277**, 242-245 (1997). https://doi.org/10.1126/science.277.5323.242

5 Armulik, A. *et al.* Pericytes regulate the blood-brain barrier. *Nature* **468**, 557-561 (2010). https://doi.org/10.1038/nature09522

6 Daneman, R., Zhou, L., Kebede, A. A. & Barres, B. A. Pericytes are required for blood-brain barrier integrity during embryogenesis. *Nature* **468**, 562-566 (2010). https://doi.org/10.1038/nature09513

7 Eilken, H. M. *et al.* Pericytes regulate VEGF-induced endothelial sprouting through VEGFR1. *Nat Commun* **8**, 1574 (2017). https://doi.org/10.1038/s41467-017-01738-3

8 Simonavicius, N. *et al.* Pericytes promote selective vessel regression to regulate vascular patterning. *Blood* **120**, 1516-1527 (2012). https://doi.org/10.1182/blood-2011-01-332338

9 Benjamin, L. E., Hemo, I. & Keshet, E. A plasticity window for blood vessel remodelling is defined by pericyte coverage of the preformed endothelial network and is regulated by PDGF-B and VEGF. *Development* **125**, 1591-1598 (1998). https://doi.org/10.1242/dev.125.9.1591

10 Hellstrom, M., Kalen, M., Lindahl, P., Abramsson, A. & Betsholtz, C. Role of PDGF-B and PDGFR-beta in recruitment of vascular smooth muscle cells and pericytes during embryonic blood vessel formation in the mouse. *Development* **126**, 3047-3055 (1999). https://doi.org/10.1242/dev.126.14.3047

11 Hirschi, K. K., Rohovsky, S. A. & D'Amore, P. A. PDGF, TGF-beta, and heterotypic cell-cell interactions mediate endothelial cell-induced recruitment of 10T1/2 cells and their differentiation to a smooth muscle fate. *J Cell Biol* **141**, 805-814 (1998). https://doi.org/10.1083/jcb.141.3.805

12 Soriano, P. Abnormal kidney development and hematological disorders in PDGF beta-receptor mutant mice. *Genes Dev* **8**, 1888-1896 (1994). https://doi.org/10.1101/gad.8.16.1888

13 Ando, K. *et al.* Conserved and context-dependent roles for pdgfrb signaling during zebrafish vascular mural cell development. *Dev Biol* **479**, 11-22 (2021). https://doi.org/10.1016/j.ydbio.2021.06.010

14 Mae, M. A. *et al.* Single-Cell Analysis of Blood-Brain Barrier Response to Pericyte Loss. *Circ Res* **128**, e46-e62 (2021). https://doi.org/10.1161/CIRCRESAHA.120.317473

15 Paredes-Gonzalez, S., Salazar-Tirado, J., Recabal-Beyer, A. & Contreras, E. G. Invertebrate glial barriers as a model for understanding blood-brain barrier

evolution. *Fluids Barriers CNS* **22**, 93 (2025). https://doi.org/10.1186/s12987-025-00694-1

16 Limmer, S., Weiler, A., Volkenhoff, A., Babatz, F. & Klambt, C. The Drosophila blood-brain barrier: development and function of a glial endothelium. *Front Neurosci* **8**, 365 (2014). https://doi.org/10.3389/fnins.2014.00365

17 Jeong, J. Y. *et al.* Functional and developmental analysis of the blood-brain barrier in zebrafish. *Brain Res Bull* **75**, 619-628 (2008). https://doi.org/10.1016/j.brainresbull.2007.10.043

18 Xie, J., Farage, E., Sugimoto, M. & Anand-Apte, B. A novel transgenic zebrafish model for blood-brain and blood-retinal barrier development. *BMC Dev Biol* **10**, 76 (2010). https://doi.org/10.1186/1471-213X-10-76

19 Quinonez-Silvero, C., Hubner, K. & Herzog, W. Development of the brain vasculature and the blood-brain barrier in zebrafish. *Dev Biol* **457**, 181-190 (2020). https://doi.org/10.1016/j.ydbio.2019.03.005

20 Umans, R. A. *et al.* CNS angiogenesis and barriergenesis occur simultaneously. *Dev Biol* **425**, 101-108 (2017). https://doi.org/10.1016/j.ydbio.2017.03.017

21 O'Brown, N. M., Megason, S. G. & Gu, C. Suppression of transcytosis regulates zebrafish blood-brain barrier function. *Elife* **8** (2019). https://doi.org/10.7554/eLife.47326

22 Li, Y. *et al.* Claudin-5a is essential for the functional formation of both zebrafish blood-brain barrier and blood-cerebrospinal fluid barrier. *Fluids Barriers CNS* **19**, 40 (2022). https://doi.org/10.1186/s12987-022-00337-9

23 Vanhollebeke, B. *et al.* Tip cell-specific requirement for an atypical Gpr124- and Reck-dependent Wnt/beta-catenin pathway during brain angiogenesis. *Elife* **4** (2015). https://doi.org/10.7554/eLife.06489

24 Guemez-Gamboa, A. *et al.* Inactivating mutations in MFSD2A, required for omega-3 fatty acid transport in brain, cause a lethal microcephaly syndrome. *Nat Genet* **47**, 809-813 (2015). https://doi.org/10.1038/ng.3311

25 Ben-Zvi, A. *et al.* Mfsd2a is critical for the formation and function of the blood-brain barrier. *Nature* **509**, 507-511 (2014). https://doi.org/10.1038/nature13324

26 Andreone, B. J. *et al.* Blood-Brain Barrier Permeability Is Regulated by Lipid Transport-Dependent Suppression of Caveolae-Mediated Transcytosis. *Neuron* **94**, 581-594 e585 (2017). https://doi.org/10.1016/j.neuron.2017.03.043

27 Eubelen, M. *et al.* A molecular mechanism for Wnt ligand-specific signaling. *Science* **361** (2018). https://doi.org/10.1126/science.aat1178

28 Parab, S. *et al.* Local angiogenic interplay of Vegfc/d and Vegfa controls brain region-specific emergence of fenestrated capillaries. *Elife* **12** (2023). https://doi.org/10.7554/eLife.86066

29 Parab, S., Quick, R. E. & Matsuoka, R. L. Endothelial cell-type-specific molecular requirements for angiogenesis drive fenestrated vessel development in the brain. *Elife* **10** (2021). https://doi.org/10.7554/eLife.64295

30 Shih, Y. H., Portman, D., Idrizi, F., Grosse, A. & Lawson, N. D. Integrated molecular analysis identifies a conserved pericyte gene signature in zebrafish. *Development* **148** (2021). https://doi.org/10.1242/dev.200189

31 Ando, K. *et al.* Clarification of mural cell coverage of vascular endothelial cells by live imaging of zebrafish. *Development* **143**, 1328-1339 (2016). https://doi.org/10.1242/dev.132654

32 Ulrich, F. *et al.* Reck enables cerebrovascular development by promoting canonical Wnt signaling. *Development* **143**, 1055 (2016). https://doi.org/10.1242/dev.136507

33 Wang, Y., Pan, L., Moens, C. B. & Appel, B. Notch3 establishes brain vascular integrity by regulating pericyte number. *Development* **141**, 307-317 (2014). https://doi.org/10.1242/dev.096107

34 Ando, K. *et al.* Peri-arterial specification of vascular mural cells from naive mesenchyme requires Notch signaling. *Development* **146** (2019). https://doi.org/10.1242/dev.165589

35 Ando, K., Ishii, T. & Fukuhara, S. Zebrafish Vascular Mural Cell Biology: Recent Advances, Development, and Functions. *Life (Basel)* **11** (2021). https://doi.org/10.3390/life11101041

36 Gall, L. G. *et al.* Zebrafish glial-vascular interactions progressively expand over the course of brain development. *iScience* **28**, 111549 (2025). https://doi.org/10.1016/j.isci.2024.111549

37 Chen, J., Poskanzer, K. E., Freeman, M. R. & Monk, K. R. Live-imaging of astrocyte morphogenesis and function in zebrafish neural circuits. *Nat Neurosci* **23**, 1297-1306 (2020). https://doi.org/10.1038/s41593-020-0703-x

38 Mayer, M. G. & Fischer, T. Microglia at the blood brain barrier in health and disease. *Front Cell Neurosci* **18**, 1360195 (2024). https://doi.org/10.3389/fncel.2024.1360195

39 Wu, S. *et al.* Il34-Csf1r Pathway Regulates the Migration and Colonization of Microglial Precursors. *Dev Cell* **46**, 552-563 e554 (2018). https://doi.org/10.1016/j.devcel.2018.08.005

40 Xu, J. *et al.* Temporal-Spatial Resolution Fate Mapping Reveals Distinct Origins for Embryonic and Adult Microglia in Zebrafish. *Dev Cell* **34**, 632-641 (2015). https://doi.org/10.1016/j.devcel.2015.08.018

41 Herbomel, P., Thisse, B. & Thisse, C. Zebrafish early macrophages colonize cephalic mesenchyme and developing brain, retina, and epidermis through a M-CSF receptor-dependent invasive process. *Dev Biol* **238**, 274-288 (2001). https://doi.org/10.1006/dbio.2001.0393

42 Gaudi, A. U. *et al.* Convergent evolution of scavenger cell development at brain borders. *Nature* (2026). https://doi.org/10.1038/s41586-025-10003-3

43 Lim, Y. W. *et al.* Trans-Endothelial Trafficking in Zebrafish: Nanobio Interactions of Polyethylene Glycol-Based Nanoparticles in Live Vasculature. *ACS Nano* (2026). https://doi.org/10.1021/acsnano.5c21042

44 Matsumoto, K. *et al.* Advanced CUBIC tissue clearing for whole-organ cell profiling. *Nat Protoc* **14**, 3506-3537 (2019). https://doi.org/10.1038/s41596-019-0240-9

45 Sinha, B. *et al.* Cells respond to mechanical stress by rapid disassembly of caveolae. *Cell* **144**, 402-413 (2011). https://doi.org/10.1016/j.cell.2010.12.031

46 Del Pozo, M. A., Lolo, F. N. & Echarri, A. Caveolae: Mechanosensing and mechanotransduction devices linking membrane trafficking to mechanoadaptation. *Curr Opin Cell Biol* **68**, 113-123 (2021). https://doi.org/10.1016/j.ceb.2020.10.008

47 Rajan, A. M., Ma, R. C., Kocha, K. M., Zhang, D. J. & Huang, P. Dual function of perivascular fibroblasts in vascular stabilization in zebrafish. *PLoS Genet* **16**, e1008800 (2020). https://doi.org/10.1371/journal.pgen.1008800

48 Tjakra, M. *et al.* Overview of Crosstalk Between Multiple Factor of Transcytosis in Blood Brain Barrier. *Front Neurosci* **13**, 1436 (2019). https://doi.org/10.3389/fnins.2019.01436

49 Boye, K. *et al.* Endothelial Unc5B controls blood-brain barrier integrity. *Nat Commun* **13**, 1169 (2022). https://doi.org/10.1038/s41467-022-28785-9

50 Ayloo, S. *et al.* Pericyte-to-endothelial cell signaling via vitronectin-integrin regulates blood-CNS barrier. *Neuron* **110**, 1641-1655 e1646 (2022). https://doi.org/10.1016/j.neuron.2022.02.017

51 Berthiaume, A. A. *et al.* Pericyte remodeling is deficient in the aged brain and contributes to impaired capillary flow and structure. *Nat Commun* **13**, 5912 (2022). https://doi.org/10.1038/s41467-022-33464-w

52 Park, D. Y. *et al.* Plastic roles of pericytes in the blood-retinal barrier. *Nat Commun* **8**, 15296 (2017). https://doi.org/10.1038/ncomms15296

53 Renshaw, S. A. & Trede, N. S. A model 450 million years in the making: zebrafish and vertebrate immunity. *Dis Model Mech* **5**, 38-47 (2012). https://doi.org/10.1242/dmm.007138

54 Vanlandewijck, M. *et al.* A molecular atlas of cell types and zonation in the brain vasculature. *Nature* **554**, 475-480 (2018). https://doi.org/10.1038/nature25739

55 Bower, N. I. *et al.* Mural lymphatic endothelial cells regulate meningeal angiogenesis in the zebrafish. *Nat Neurosci* **20**, 774-783 (2017). https://doi.org/10.1038/nn.4558

56 Hogan, B. M. *et al.* Ccbe1 is required for embryonic lymphangiogenesis and venous sprouting. *Nat Genet* **41**, 396-398 (2009). https://doi.org/10.1038/ng.321

57 Jin, S. W., Beis, D., Mitchell, T., Chen, J. N. & Stainier, D. Y. Cellular and molecular analyses of vascular tube and lumen formation in zebrafish. *Development* **132**, 5199-5209 (2005). https://doi.org/10.1242/dev.02087

58 Traver, D. *et al.* Transplantation and in vivo imaging of multilineage engraftment in zebrafish bloodless mutants. *Nat Immunol* **4**, 1238-1246 (2003). https://doi.org/10.1038/ni1007

59 Asakawa, K. *et al.* Genetic dissection of neural circuits by Tol2 transposon-mediated Gal4 gene and enhancer trapping in zebrafish. *Proc Natl Acad Sci U S A* **105**, 1255-1260 (2008). https://doi.org/10.1073/pnas.0704963105

60 Davis, A. E., Castranova, D. & Weinstein, B. M. Rapid Generation of Pigment Free, Immobile Zebrafish Embryos and Larvae in Any Genetic Background Using CRISPR-Cas9 dgRNPs. *Zebrafish* **18**, 235-242 (2021). https://doi.org/10.1089/zeb.2021.0011

61 Suster, M. L., Sumiyama, K. & Kawakami, K. Transposon-mediated BAC transgenesis in zebrafish and mice. *BMC Genomics* **10**, 477 (2009). https://doi.org/10.1186/1471-2164-10-477

62 Bussmann, J. & Schulte-Merker, S. Rapid BAC selection for tol2-mediated transgenesis in zebrafish. *Development* **138**, 4327-4332 (2011). https://doi.org/10.1242/dev.068080

63 Pugach, E. K., Li, P., White, R. & Zon, L. Retro-orbital injection in adult zebrafish. *J Vis Exp* (2009). https://doi.org/10.3791/1645

64 Okuda, K. S., Baek, S. & Hogan, B. M. Visualization and Tools for Analysis of Zebrafish Lymphatic Development. *Methods Mol Biol* **1846**, 55-70 (2018). https://doi.org/10.1007/978-1-4939-8712-2_4

65 Lim, Y. W. *et al.* Caveolae Protect Notochord Cells against Catastrophic Mechanical Failure during Development. *Curr Biol* **27**, 1968-1981 e1967 (2017). https://doi.org/10.1016/j.cub.2017.05.067

66 Schindelin, J. *et al.* Fiji: an open-source platform for biological-image analysis. *Nat Methods* **9**, 676-682 (2012). https://doi.org/10.1038/nmeth.2019

67 Isogai, S., Horiguchi, M. & Weinstein, B. M. The vascular anatomy of the developing zebrafish: an atlas of embryonic and early larval development. *Dev Biol* **230**, 278-301 (2001). https://doi.org/10.1006/dbio.2000.9995